

Communication-Efficient and Differentially Private Vertical Federated Learning with Zeroth-Order Optimization

Jianing Zhang, *Student Member, IEEE*, Evan Chen, *Student Member, IEEE*, Dong-Jun Han, *Member, IEEE*, Chaoyue Liu, *Member, IEEE*, Christopher G. Brinton, *Senior Member, IEEE*

Abstract—Vertical Federated Learning (VFL) enables collaborative model training across feature-partitioned devices, yet its reliance on device-server information exchange introduces significant communication overhead and privacy risks. Downlink communication from the server to devices in VFL exposes gradient-related signals of the global loss that can be leveraged in inference attacks. Existing privacy-preserving VFL approaches that inject differential privacy (DP) noise on the downlink have the natural repercussion of degraded gradient quality, slowed convergence, and excessive communication rounds. In this work, we propose DPZV, a communication-efficient and differentially private ZO-VFL framework with tunable privacy guarantees. Based on zeroth-order (ZO) optimization, DPZV injects calibrated scalar-valued DP noise on the downlink, significantly reducing variance amplification while providing equivalent protection against targeted inference attacks. Through rigorous theoretical analysis, we establish convergence guarantees comparable to first-order DP-SGD, despite relying solely on ZO estimators, and prove that DPZV satisfies (ϵ, δ) -DP. Extensive experiments demonstrate that DPZV consistently achieves a superior privacy–utility tradeoff and requires fewer communication rounds than existing DP-VFL baselines under strict privacy constraints ($\epsilon \leq 10$).

Index Terms—Vertical Federated Learning, Differential Privacy, Distributed Optimization

I. INTRODUCTION

Vertical Federated Learning (VFL) has emerged as a compelling paradigm for distributed training over edge and wireless systems where devices hold complementary features for the same data samples [1]–[3]. Such vertical feature partitioning naturally arises in many applications. For example, in wireless sensor networks, spatially-distributed nodes may each collect local environmental measurements treated as features in a learning task [4]–[7]. In other distributed setups, devices may only be capable of storing a portion of the features due to strict memory budgets or security concerns [8], [9]. In these settings, VFL enables flexible model deployment by allowing learning to be distributed across devices with only a server/fusion center storing and processing the full model.

In most VFL systems, different devices holding partial features exchange intermediate gradients or embeddings with the server for aggregation [2], [10], [11]. This is in contrast to conventional (horizontal) FL [4], [12]–[14], where each device holds a full feature vector for a subset of the samples, and updates are exchanged on the full model. The result is a different

J. Zhang, E. Chen, C. Liu, and C. Brinton are with the Elmore Family School of Electrical and Computer Engineering, Purdue University, West Lafayette, IN 47907, USA. Email: {zhan4670, chen4388, cyliu, cgb}@purdue.edu.

D.-J. Han is with the Department of Computer Science and Engineering, Yonsei University, Seoul 03722, Republic of Korea. Email: djh@yonsei.ac.kr.

communication pattern in VFL, where information exchange typically occurs with respect to smaller submodel partitions rather than through full model updates. Still, communication efficiency is a pressing issue in VFL, influenced heavily by the feature dimensionality and training procedure [9], [15].

Beyond efficiency concerns, VFL’s reliance on transmitting intermediate results introduces privacy concerns. Recent studies have shown that adversaries can exploit communicated information to infer sensitive attributes (feature inference attacks) [16], [17] or even recover labels (label inference attacks) [18], [19] and leverage them in e.g., backdoor attacks [20]. Under the commonly adopted honest-but-curious threat model, these risks are particularly pronounced on the downlink, where gradient-related signals directly encode label-dependent information. Therefore, protecting downlink communication is essential for safeguarding privacy in VFL.

Unfortunately, existing mitigation measures for these privacy concerns often harm model performance and further exacerbate the communication burden of VFL. Similar to conventional FL, VFL methods often protect gradients by injecting calibrated noise vectors using differential privacy (DP) mechanisms [2], [21]–[23]. However, such noise inevitably degrades gradient quality, leading to slower convergence and thus requiring more communication rounds to reach a target accuracy. Consequently, privacy protection and communication efficiency are tightly coupled in DP-enhanced VFL (DP-VFL): stronger privacy requirements for a fixed target model quality typically translate into heavier communication costs.

A. Zeroth-Order VFL

Zero-order (ZO) optimizers [24], [25] offer a compelling foundation for building private and efficient solutions to VFL [21], [26]. Migrating from first-order gradient descent-based methods to zero-order VFL (ZO-VFL) is motivated by two key observations. First, ZO methods eliminate explicit gradient transmission in the backward phase, substantially reducing information leakage and providing a stronger baseline defense against label inference attacks [26]. Second, ZO enables optimization using only function evaluations. As a result, the backward communication in ZO-VFL consists of scalar-valued feedback rather than high-dimensional gradients. This significantly limits the dimensionality of information transmitted and potentially revealed per downlink interaction.

However, ZO-VFL alone does not fully resolve privacy concerns. Despite the absence of explicit gradients, malicious devices can still approximate gradients from perturbation-based scalar feedback, leaving ZO-VFL vulnerable to inference attacks. Moreover, while recent work [21] has quantified

an inherent differential privacy provided by ZO methods, these levels are typically insufficient when strong DP guarantees are needed [27]. Importantly, these DP levels are also not adjustable, limiting their practicality in real-world deployments that require controllable privacy guarantees.

These limitations lead to the central question of this work:

How can VFL obtain communication efficiency advantages as in ZO-VFL while preserving controllable privacy levels as in DP-VFL?

To answer this question, we observe that achieving communication efficiency in DP-VFL is fundamentally tied to obtaining a favorable privacy-accuracy tradeoff, since improved convergence behavior directly translates into fewer communication rounds needed to reach a target accuracy. However, accomplishing this goal faces two key challenges. First, *existing approaches for enforcing differential privacy in VFL commonly inject noise into the forward embeddings* [2], [22], which are typically high-dimensional. As a result, the injected noise induces substantial variance amplification and significantly slows convergence, particularly under tight privacy budgets. Second, *ZO optimization methods rely on inherently noisy gradient estimators and are generally known to converge more slowly than first-order methods* [28]. When combined with additional DP noise, this effect can be further amplified, potentially leading to severe performance degradation and an increased number of communication rounds.

B. Summary of Contributions

In this work, we propose DPZV, a VFL methodology which achieves communication efficiency and controllable differential privacy concurrently. Instead of perturbing the forward embeddings, our method injects scalar-valued DP noise into the backward information. Intuitively, injecting scalar noise preserves the directional structure of the ZO gradient estimator and introduces far less distortion than vector-valued perturbations, enabling more accurate updates and faster convergence under the same privacy budget. We show in Sec. VI that this design achieves the same level of protection against targeted label and feature inference attacks as forward perturbations, while significantly reducing noise dimensionality.

Through both theoretical analysis and extensive experiments, we demonstrate that our approach provides faster convergence than existing methods under a fixed privacy budget, incurring the lowest total communication cost to reach a target accuracy. More specifically, our contributions are as follows:

- DPZV is the first VFL methodology that enables tunable differential privacy while maintaining communication efficiency. Unlike existing DP-VFL methods that inject high-dimensional noise into forward embeddings, DPZV perturbs only the scalar-valued backward information. This design preserves privacy guarantees while substantially reducing variance in the gradient estimation, leading to faster convergence and fewer required communication rounds. By eliminating gradient transmission, DPZV is particularly well suited for privacy-critical and communication-constrained deployments (Sec. IV).

- We provide a rigorous theoretical analysis establishing both convergence and privacy guarantees for DPZV. Specifically, we show that DPZV achieves a convergence rate to a stationary point on the same order as first-order DP methods, despite using less precise ZO estimators. This result demonstrates that the conventional gap in convergence speed between ZO and first-order methods diminishes in the DP-VFL setting. Furthermore, we prove that our method satisfies (ϵ, δ) -DP, confirming its ability to provide an adjustable privacy control mechanism while retaining communication efficiency (Sec. V, VI).
- Through experiments on four benchmark datasets, we verify that DPZV obtains robust convergence performance under strict privacy budgets. In particular, while the baseline algorithms experience a steep performance degradation and/or increase in communication rounds as the privacy level increases, we find that DPZV consistently maintains faster convergence to a target accuracy across all tasks, underscoring an elevated privacy-utility-cost tradeoff. In addition to a lower total communication cost, we find that DPZV reduces the required memory overhead for training large models (Sec. VII).

II. RELATED WORK

A. Vertical Federated Learning

VFL enables collaborative training across entities (e.g., organizations or, in our case, wireless devices) with vertically partitioned features. Early VFL frameworks focused on simple device-side models such as logistic regression and linear models [1]. These methods prioritized simplicity, but lacked expressiveness for complex tasks. To address this limitation, larger device-side models like deep neural networks (DNNs) were adopted [2], [3], [22].

A key challenge in VFL is the communication overhead incurred during training. One popular mechanism for reducing communication overhead is by allowing for multiple local updates in-between aggregations. In this respect, [29] introduced FedBCD, which allows devices to perform multiple gradient iterations in VFL before synchronization. Similarly, Flex-VFL [3] proposed a flexible strategy offering varying local update counts per party, constrained by a communication timeout. VIMADMM [22] adopted an ADMM-based approach to enable multiple local updates in VFL. On the other hand, Asynchronous VFL methods (e.g., FDML [30], VAFL [2]) decouple coordination, allowing devices to update models independently, thus improving scalability. However, in first-order methods, the backward pass through neural networks typically imposes communication overhead, while our ZO-based approach significantly reduces the cost associated with backward propagation.

Privacy guarantees are another critical challenge for VFL adoption. Some VFL architectures use crypto-based privacy-preserving techniques such as Homomorphic Encryption (HE) [31], but lack formal assurances. In contrast, DP provides rigorous mathematical protection. Key DP-based methods include VAFL [2], which injects Gaussian noise into device embeddings during forward propagation to achieve Gaussian DP,

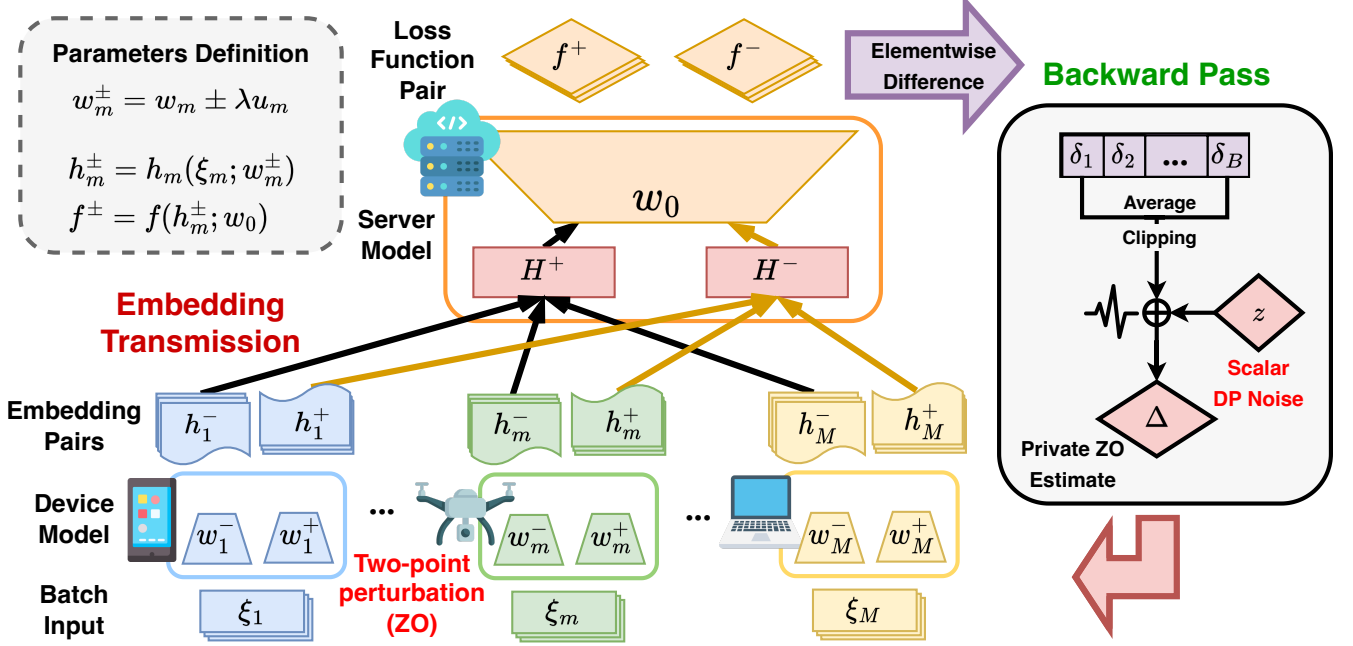


Fig. 1: Overview of the training procedure in DPZV. Each device perturbs its local model parameters in two random directions to generate a pair of embeddings, which are then transmitted to the server. The server computes the corresponding function evaluations and applies an elementwise difference to approximate the zeroth-order (ZO) gradient. To ensure differential privacy, scalar-valued Gaussian noise is injected into the aggregated ZO estimate. Unlike traditional vector-valued noise in standard DP algorithms, scalar noise is significantly smaller in norm, thereby preserving model utility even under stringent privacy budgets.

and VIMADMM [22], which perturbs linear model parameters with bounded sensitivity, ensuring DP guarantees for convex settings. Our work overcomes challenges in developing such methods for the ZO setting.

B. Zeroth-Order Optimization

Recent research has explored ZO optimization within VFL to accommodate resource-constrained devices with non-differentiable models and to reduce gradient leakage. Early work like ZOO-VFL [26] adopted a naive ZO approach throughout VFL training but provided no DP guarantees. VFL-CZOFO [21] introduced a cascaded hybrid optimization method, combining zeroth-order and first-order updates, which leveraged intrinsic noise from ZO for limited privacy. However, its DP level was not adjustable, resulting in insufficient protection.

More recently, MeZO [32] proposed a memory-efficient ZO algorithm. Building upon these ideas, DPZero [33] and DPZO [34] introduced private ZO variants offering baseline privacy features. However, these methods are designed for centralized settings and cannot be directly extended to the VFL paradigm. Extending beyond previous efforts to combine ZO optimization with VFL, we further integrate a controllable differential privacy mechanism, achieving an elevated trade-off between privacy and model performance.

III. PRELIMINARIES

A. System Model for VFL

We consider a VFL framework with one server and M devices. In VFL, data is vertically partitioned between devices, with each device holding different features of the data.

Suppose we have a dataset \mathcal{D} with D samples: $\mathcal{D} = \{\xi_i | i = 1, 2, \dots, D\}$. Each data sample ξ_i can be partitioned into M portions distributed throughout all devices, where the data sample on machine m with ID i is denoted as $\xi_{m,i}$, hence $\xi_i = [\xi_{1,i}, \xi_{2,i}, \dots, \xi_{M,i}]^\top$. The server is numbered as machine 0 and holds the label data $\mathbf{Y} = \{y_i | i = 1, 2, \dots, D\}$.

The devices and the server aim to jointly train a machine learning model parameterized by \mathbf{w} . The global model comprises local models on each party parameterized by w_m , with $m = 0, 1, \dots, M$ being the ID of the machine. To protect privacy, devices do not communicate with each other regarding data or model parameters. Instead, all devices communicate directly with the server regarding their local model's outputs, which we term as local embeddings. If we denote the local embedding of device m as $h_{m,i} := h(w_m; \xi_{m,i})$, the objective of the VFL framework can be seen as minimizing the following function:

$$F(\mathbf{w}; \mathcal{D}, \mathbf{Y}) := \frac{1}{D} \sum_{i \in [D]} \mathcal{L}(w_0, h_{1,i}, h_{2,i}, \dots, h_{M,i}; y_i) \quad (1)$$

where \mathcal{L} is the loss function for a datum ξ_i and its corresponding label y_i . For the simplicity of notation, we define the loss function w.r.t a specific model parameter and datum as

$$f(\mathbf{w}; \xi_i) := \mathcal{L}(w_0, h_{1,i}, h_{2,i}, \dots, h_{M,i}; y_i) \quad (2)$$

Memory-Efficient Zeroth-Order Optimizer. We introduce the two-point gradient estimator [35], which will serve as our zeroth-order gradient estimator throughout this paper. Let u be uniformly sampled from the Euclidean sphere $\sqrt{d}\mathbb{S}^{d-1}$ and $\lambda > 0$ be the smoothing factor. For a single datum ξ sampled

from the whole dataset \mathcal{D} , the two-point gradient estimator is defined as

$$g(x; \xi) = \frac{f(x + \lambda u; \xi) - f(x - \lambda u; \xi)}{2\lambda} u \quad (3)$$

To further reduce the memory overhead on device, we adopt the `MeZO` methodology [32] for our ZO Optimization, which requires only the same memory as the model itself for training. We investigate the memory reduction of this estimator in Section VII.

B. Differential Privacy and DP-SGD

DP provides a principled framework for protecting individual data in statistical analysis and machine learning. Formally, we adopt the standard (ϵ, δ) -DP definition:

Definition III.1 $((\epsilon, \delta)$ -Differential Privacy). A randomized algorithm $\mathcal{M} : \mathcal{X}^n \rightarrow \Theta$ is said to satisfy (ϵ, δ) -differential privacy if for any neighboring datasets $X, X' \in \mathcal{X}^n$ that differ by only one individual's data, and for any subset of outputs $E \subseteq \Theta$, we have

$$\mathbb{P}[\mathcal{M}(X) \in E] \leq e^\epsilon \mathbb{P}[\mathcal{M}(X') \in E] + \delta. \quad (4)$$

One of the most widely adopted private training algorithms is Differentially Private Stochastic Gradient Descent (DP-SGD), which operates by clipping an intermediate result and injecting Gaussian noise during each model update. Specifically, given a minibatch B_t at iteration t , DP-SGD performs the following steps:

- 1) Clip individual gradients:
 $\bar{g}_i = \nabla \ell(\theta_t, x_i), \quad \tilde{g}_i = \bar{g}_i / \max\left(1, \frac{\|\bar{g}_i\|_2}{C}\right)$
- 2) Add Gaussian noise:
 $\tilde{g}_t = \frac{1}{|B_t|} \left(\sum_{i \in B_t} \tilde{g}_i + \mathcal{N}(0, \sigma^2 C^2 \mathbf{I}) \right)$
- 3) Update model: $\theta_{t+1} = \theta_t - \eta_t \tilde{g}_t$

C. Challenges and Motivation

Existing approaches [2], [22] integrate DP with first order VFL by injecting DP noise in the forward embedding. In centralized or horizontally federated learning, DP-SGD achieves privacy by adding noise to the backward gradients. However, extending these strategies to ZO optimization introduces new challenges. First, *due to the distributed nature of VFL, DP guarantees must be enforced during the downlink process between the cloud and devices, so as to prevent malicious devices from mounting label inference attacks*. In both cases, the noise must match the dimensionality of the protected vector (embedding or gradient), often resulting in high-dimensional noise. This situation is further exacerbated by the second factor: in ZO methods, gradients are approximated through multiple forward evaluations, making them inherently noisy. Adding a *high-dimensional* noise vector as in standard DP-SGD further amplifies this inaccuracy.

A key advantage of adopting ZO optimization, however, lies in its communication efficiency in the backward pass: only a scalar value, rather than a full gradient vector, needs to be exchanged. This observation enables *a more efficient*

privacy mechanism—injecting scalar noise rather than high-dimensional noise. Building on this insight, we propose Differentially Private Zeroth-Order Vertical Federated Learning (DPZV), a framework that achieves tunable differential privacy through calibrated scalar noise injection. This design allows for a favorable privacy-utility trade-off in ZO-based VFL, particularly under tight privacy budgets. Unlike first-order VFL methods, which typically add noise to forward embeddings, DPZV introduces noise in the backward pass, targeting the most exploited leakage pathway in VFL: label inference from gradients. A broader discussion of privacy implications is provided in Section VI.

IV. METHODOLOGY

In this section, we describe the overall training procedure of DPZV. Based on (1), the objective is to collaboratively minimize the global objective function across all devices. The devices hold disjoint features of the same data records, and the server holds the label data. The training procedure proceeds in two iterative steps.

A. Device Update and Forward Communication

The sampled devices compute local information and transmit it to the server. We define the device-server communication as *forward communication*.

Training Procedure. Each device m maintaining its own local communication round t_m , while the server tracks a global round t . Whenever the server receives information from a device, it increments t . Upon receiving an update from the server, the device synchronizes by setting $t_m = t$, capturing the latest state. This asynchronous mechanism allows devices to progress without waiting for stragglers, improving throughput and minimizing idle time. The server maintains a copy of the latest local embeddings $\tilde{h}_{m,i}^t$ for all devices $m \in [M]$ and data samples $\xi_i \in \mathcal{D}$. Due to the asynchronous nature of the algorithm, these copies may be stale, as they do not always reflect the most up-to-date model parameters of the devices. Let $\tilde{t}_{m,i}$ denote the device time when the server last updated $\tilde{h}_{m,i}^t$. The delay at server communication round t can then be expressed as $\tau_m^t = t_m - \tilde{t}_{m,i}$, where the delayed model parameters are defined as:

$$\tilde{h}^t = \{w_1^{t_1 - \tau_1^t}, \dots, w_M^{t_M - \tau_M^t}\}, \quad \tilde{w}^t = \{w_0^t, \tilde{h}^t\}. \quad (5)$$

Local Embedding Finite Differences. For each global iteration t , a device m is activated, and it samples a mini-batch $\mathcal{B}_m^{t_m} \in \mathcal{D}$ and the corresponding IDs $\mathcal{I}_m^{t_m}$. To approximate gradients via zeroth-order finite differences, device m computes two perturbed local embeddings for the mini-batch,

$$\begin{aligned} \{h_{m,i}^{t_m+}\}_{i \in \mathcal{I}_m^{t_m}} &= \{h(w_m^{t_m} + \lambda_m \mathbf{u}_m^{t_m}; \xi_{m,i})\}_{i \in \mathcal{I}_m^{t_m}}, \\ \{h_{m,i}^{t_m-}\}_{i \in \mathcal{I}_m^{t_m}} &= \{h(w_m^{t_m} - \lambda_m \mathbf{u}_m^{t_m}; \xi_{m,i})\}_{i \in \mathcal{I}_m^{t_m}} \end{aligned} \quad (6)$$

where $\mathbf{u}_m^{t_m}$ is sampled uniformly at random from the Euclidean sphere $\sqrt{d_m} \mathbb{S}^{d_m-1}$, and λ_m is a smoothing parameter that controls the step size of perturbation. These two perturbed embeddings serve as “positive” and “negative” perturbations of its local parameters, which are forwarded to the server for further computation.

Algorithm 1: DPZV: Differentially Private Zeroth-Order Vertical Federated Learning

Input : Data \mathcal{D} , batch size B , learning rate η_m , total iteration T , smoothing parameter $\lambda_m > 0$, clipping threshold $C > 0$, privacy parameter σ_{dp}

Output: Parameter w_0, w_m for all parties $m \in [M]$

- 1 Initialize w_0, w_m and set $t, t_m = 0$ for all parties
- 2 **for** $t = 1, \dots, T$ **do**
- 3 Sample ready-to-update device $m \in \{1, \dots, M\}$.
- 4 device m samples a mini-batch $\mathcal{B}_m^{t_m}$ with corresponding IDs $\mathcal{I}_m^{t_m}$.
- 5 device m computes perturbed local embeddings:
- 6 $\{h_{m,i}^{t_m+}\}_{i \in \mathcal{I}_m^{t_m}} = \{h(w_m^{t_m} + \lambda_m \mathbf{u}_m^{t_m}; \xi_{m,i})\}_{i \in \mathcal{I}_m^{t_m}},$
- 7 $\{h_{m,i}^{t_m-}\}_{i \in \mathcal{I}_m^{t_m}} = \{h(w_m^{t_m} - \lambda_m \mathbf{u}_m^{t_m}; \xi_{m,i})\}_{i \in \mathcal{I}_m^{t_m}}$
- 8 **(Forward)** Device transmits embeddings to server.
- 9 Server computes Δ_m^t , and updates via ZO Optimization:

$$\delta_{m,i}^{t,t_m} = \frac{\tilde{f}(w_0, h_{m,i}^{t_m+}; y_i) - \tilde{f}(w_0, h_{m,i}^{t_m-}; y_i)}{\lambda_m},$$

$$\Delta_m^t = \frac{1}{B} \sum_{i \in \mathcal{I}_m^{t_m}} \text{clip}_C(\delta_{m,i}^{t,t_m}) + z_m^t.$$
- 10 **(Backward)** Device receives Δ_m^t .
- 11 Device performs local update:

$$\mathbf{w}_m \leftarrow \mathbf{w}_m - \eta_m \Delta_m^t \mathbf{u}_m^{t_m}.$$
- 12 Device update local time stamp $t_m = t$.

B. Server Update and Backward Communication

The server updates the global model and transmit global updates to the device. We define the server-device communication as *backward communication*.

Server Side ZO Computation. After the server receives the local embeddings $h_{m,i}^{t_m}$ from device m , it updates its embeddings copy and do computation. For each embedding pair $\{h_{m,i}^{t_m+}, h_{m,i}^{t_m-}\}$, it computes the difference in loss function \mathcal{L} caused by perturbation, divided by the smooth parameter λ_m . Specifically, we define¹:

$$\delta_{m,i}^{t,t_m} = \frac{\tilde{f}(w_0, h_{m,i}^{t_m+}; y_i) - \tilde{f}(w_0, h_{m,i}^{t_m-}; y_i)}{\lambda_m}, \quad (7)$$

Scalar DP Noise Injection. To ensure controllable privacy, the server then clips each $\delta_{m,i}^t$ by a threshold C to bound sensitivity: $\text{clip}_C(\delta_{m,i}^{t,t_m}) = \min\{\delta_{m,i}^{t,t_m}, C\}$. It then samples noise z_m^t from a Gaussian distribution $\mathcal{N}(0, \sigma_{dp}^2)$. This noise is added to the mean of the per-sample-clipped updates, yielding a differentially private gradient-like quantity:

$$\Delta_m^t = \frac{1}{B} \sum_{i \in \mathcal{I}_m^{t_m}} \text{clip}_C(\delta_{m,i}^{t,t_m}) + z_m^t. \quad (8)$$

¹We slightly abuse the notation, and define $\tilde{f}(w_0, h_{m,i}^{t_m\pm}; y_i) = \mathcal{L}(w_0, \tilde{h}_{1,i}^t, \dots, h_{m,i}^{t_m\pm}, \dots, \tilde{h}_{M,i}^t; y_i)$, where we treat \tilde{f} as a function of the server parameter w_0 and the perturbed local embeddings.

The server then performs a backward communication and sends Δ_m^t to device m . The server then updates its global model through two possible operations: *i*) ZO Optimization, $w_0 \leftarrow w_0 - \eta_0 g(w_0; \xi_i)$ (defined in (3)); or *ii*) stochastic gradient descent (SGD), $w_0 \leftarrow w_0 - \eta_0 \nabla_{w_0} F(w; \xi_i)$,

depending on the constraints on computation resources. The adopted ZO update methodology is explained in Sec III.

On the device side, upon receiving Δ_m^t , device m updates its local parameter w_m with learning rate η_m :

$$\mathbf{w}_m \leftarrow \mathbf{w}_m - \eta_m \Delta_m^t \mathbf{u}_m^{t_m}, \quad (9)$$

where $\mathbf{u}_m^{t_m}$ is the same vector used for local perturbation. Our method is well-suited for resource-constrained environments, such as edge devices with limited VRAM or computation power, while still maintaining robust performance and scalability in VFL settings. We summarize the pipeline above in Algorithm 1.

V. CONVERGENCE ANALYSIS

In this section, we provide the convergence analysis for DPZV. For brevity, we define the following notations: $F^t = F(\mathbf{w}^t) := F(\mathbf{w}^t; \mathcal{D}, \mathbf{Y})$, and $f(\mathbf{w}; \xi_i)$ as defined in (2). We make the following standard assumptions²:

Assumption V.1 (Properties of loss function). The VFL objective function F is bounded from below, the function $f(\mathbf{w}; \xi_i)$ is ℓ -Lipschitz continuous and L -Smooth for every $\xi_i \in \mathcal{D}$.

Assumption V.2 (System boundedness). The following system dynamics are bounded: 1) *Stochastic Noise*: The variance of the stochastic first order gradient is upper bounded in expectation: $\mathbb{E}[\|\nabla_{\mathbf{w}} f(\mathbf{w}; \xi) - \nabla_{\mathbf{w}} F(\mathbf{w})\|^2] \leq \sigma_s^2$. 2) *Time Delay*: The parameter delay τ_m^t is upper bounded by a constant τ : $\tau^t \leq \tau, \quad \forall m, t$.

Assumption V.3 (Independent Participation). Under an asynchronous update system, the probability of one device participating in one communication round is independent of other devices and satisfies: $\mathbb{P}(\text{device } m \text{ uploading}) = q_m$.

A. Convergence Guarantee and Discussion

We now present the main theorem that provides convergence guarantee for DPZV:

Theorem V.4. Under assumption V.1-V.3, define $\mathcal{F} = \mathbb{E}[F^0 - F^T]$. Denote $q_* = \min_m q_m$, $d_* = \max_m d_m$ where d_m represent the dimension of model parameters on device m , let all step sizes satisfy: $\eta_0 = \eta_m = \eta \leq \min\{\frac{1}{\sqrt{T}d_*}, \frac{B}{4L(B+8d_0)+8\gamma_1(2d_m+B)}\}$, let the smoothing parameter λ satisfy: $\lambda \leq \frac{1}{Ld\sqrt{T}}$, and let the clipping level C satisfy: $C \geq \max\{0, \frac{1}{2}L\lambda d - \ell\sqrt{8\log(2\sqrt{2\pi})}\}$. Then, for any

²Assumption V.1 and V.2 are standard in VFL and ZO literature [3], [21]. We follow [33] to make the ℓ -Lipschitz assumption in order to bound the probability of clipping. Assumption V.3 is common when dealing with asynchronous participation [2], and can be satisfied when the activations of devices follow independent Poisson processes.

given global iteration $T \geq 1$, we have the following upper bound on the gradient norm:

$$\begin{aligned} & \frac{1}{T} \sum_{t=0}^{T-1} \mathbb{E} \left[\|\nabla_{\mathbf{w}} F(\mathbf{w}^t)\|^2 \right] \\ & \leq \mathcal{O} \left(\frac{\mathcal{F} \sqrt{d_*}}{\sqrt{T}} + \frac{d_*}{T} + \frac{(\sigma_s^2/B + \sigma_{dp}^2) \sqrt{d_*}}{\sqrt{T}} \right. \\ & \quad \left. + \frac{C^2 \sqrt{d_*}}{(\exp(C^2) - 1) B \sqrt{T}} \right), \end{aligned} \quad (10)$$

Discussion. The first term is influenced by the model's initialization, F^0 . This term also enjoys the same rate as ZO optimization in the centralized case [28]. The second term $\mathcal{O}(\frac{d_*}{T})$ is a standard term for ZOO methods based on the usage of ZO estimator updates. The third term captures the impact of various noise sources in the learning system. Here, σ_s^2/B represents the noise introduced by stochastic gradients, and σ_{dp}^2 corresponds to the variance of the injected DP noise. While reducing σ_{dp}^2 improves utility, it comes at the cost of weakening privacy guarantees. Consequently, this term encapsulates the fundamental trade-off between model performance, computational cost, and privacy budget. The fourth term, quantifies the impact of the gradient clipping operation on convergence. As C increases, increases, this term diminishes, effectively recovering the non-private case in the limit. However, the noise variance σ_{dp}^2 also scales linearly with C , which can impede overall convergence. This trade-off underscores the importance of carefully tuning the sensitivity level to balance privacy preservation and learning efficiency.

By combining the convergence analysis in Theorem V.4 with the privacy mechanism in Section VI, we obtain the following corollary, which characterizes the privacy-utility tradeoff of DPZV.

Corollary V.5. *Under the assumptions of Theorem V.4, consider the differentially private mechanism described in Section VI, where the variance of the injected DP noise is chosen as $\sigma_{dp} = \frac{2C\sqrt{T}}{D\mu}$. If the total number of global iterations is selected as*

$$T = \mathcal{O} \left(\frac{D^2 \mu^2 \sqrt{d}}{C^2} \left(\mathcal{F} + \frac{\sigma^2}{B} + \frac{C^2}{e^{C^2} - 1} \right) \right), \quad (11)$$

then the convergence bound in Theorem V.4 implies

$$\frac{1}{T} \sum_{t=0}^{T-1} \mathbb{E} \left[\|\nabla \mathcal{F}(\mathbf{w}^t)\|^2 \right] = \mathcal{O} \left(\frac{\sqrt{d}}{D\mu} \right). \quad (12)$$

Discussion. Corollary V.5 shows that, under differential privacy constraints, the proposed zeroth-order method attains the same asymptotic privacy–utility tradeoff as differentially private first-order methods, such as DP-SGD [36]. This result highlights an important contrast with the non-private setting: although zeroth-order optimization generally exhibits slower convergence than first-order methods, the proposed DP noise injection strategy reshapes the dominant error terms in the convergence analysis, allowing zeroth-order methods to achieve comparable asymptotic guarantees.

B. Proof of Theoretical Results

In this part, we briefly describe the main steps behind the main convergence theorem V.4.

The proof of the theorem follows the standard smoothness-based descent framework for non-convex optimization. However, the convergence is affected by stochastic sampling, zeroth-order perturbations, differential privacy noise, gradient clipping and communication delays, and we need to bound them. The following lemmas solve these questions, and the full details are relegated to Appendix A.

We first introduce the following lemma, which bound how much the ZO estimator is biased from the ground truth gradient.

Lemma V.6. *Let $g(\mathbf{w})$ be the zeroth-order gradient estimator defined as in (24), with $f(\mathbf{w})$ being the loss function. We define the smoothed function $f_\lambda(\mathbf{w}) = \mathbb{E}_{\mathbf{u}}[f(\mathbf{w} + \lambda \mathbf{u})]$, where \mathbf{v} is uniformly sampled from the Euclidean ball $\sqrt{d} \mathbb{B}^d = \{\mathbf{w} \in \mathbb{R}^d \mid \|\mathbf{w}\| \leq \sqrt{d}\}$. The following properties hold:*

- (i) $f_\lambda(\mathbf{w})$ is differentiable and $\mathbb{E}_{\mathbf{u}}[g(\mathbf{w})] = \nabla f_\lambda(\mathbf{w})$.
- (ii) If $f(\mathbf{w})$ is L -smooth, we have that

$$\|\nabla f(\mathbf{w}) - \nabla f_\lambda(\mathbf{w})\| \leq \frac{L}{2} \lambda d^{3/2}, \quad (13)$$

$$|f(\mathbf{w}) - f_\lambda(\mathbf{w})| \leq \frac{L}{2} \lambda^2 d, \quad (14)$$

and

$$\mathbb{E}_{\mathbf{u}}[\|g_\lambda(\mathbf{w})\|^2] \leq 2d \cdot \|\nabla f(\mathbf{w})\|^2 + \frac{L^2}{2} \lambda^2 d^3. \quad (15)$$

This is the standard result of zeroth-order optimization. The proof of the Lemma is given by [24]. In typical differential privacy algorithm, we need to clip the gradient to control the sensitivity, which is also the case in our algorithm. To control the effect of clipping, the following lemma evaluates the probability that clipping happens, so that we can take expectation w.r.t. the clipping effect in the future.

Lemma V.7. *Let Q be the event that clipping happened for a sample ξ , d be the model dimension, and L, ℓ be the Lipschitz and smooth constant as defined in assumption V.1. For $\forall C_0 > 0$, if the clipping threshold C follows $C \geq C_0 + L\lambda d/2$, we have the following upper bound for the probability of clipping:*

$$P = \mathbb{P}(Q) \leq \underbrace{2\sqrt{2\pi} \exp(-\frac{C_0^2}{8\ell^2})}_{\Xi} \quad (16)$$

Furthermore, we have the following lemma that bounds the variance of the private zeroth-order gradient estimator, leveraging the auxiliary lemmas, Lemma V.6 and V.7. It addresses the effect of stochastic sampling, zeroth-order bias, gradient clipping and DP noise at the same time.

Lemma V.8. *Let $\check{G}_m^t(\mathbf{w}^t)$ be the Differential Private Zeroth-order Gradient without delay. We can bound the variance of $\check{G}_m^t(\mathbf{w}^t)$ in expectation, with the expectation taken on random direction \mathbf{u} , DP noise z , and clipping event Q :*

$$\text{Var}(\check{G}_m^t(\mathbf{w}^t)) \leq$$

$$\begin{aligned} & \frac{1-P}{B}(2d_m\mathbb{E}\|\nabla_{w_m}F(\mathbf{w}^t)\|^2 + 2d_m\sigma_s^2 + \frac{L^2}{2}\lambda^2d_m^3) \\ & + \frac{P}{B}C^2d_m - \frac{(1-P)^2}{B}\mathbb{E}\|\nabla_{w_m}F_\lambda(\mathbf{w}^t)\|^2 + \sigma_{dp}^2d_m \end{aligned} \quad (17)$$

Using the lemma above, we are ready to derive the proof for Theorem V.4.

Proof for Theorem V.4. We start the proof by using the ℓ -Lipschitz property in Assumption V.1, which is the common practice in non-convex optimization. We then taking expectation w.r.t. the random sampling, clipping event and ZO perturbation, where we utilized Lemma V.6 and V.7. Finally, we use the result in Lemma V.8 to bound the variance terms. The result is the following one-step descent Lemma V.9, which quantifies the decrease of the objective function in a single communication round.

Lemma V.9 (Model Update With Delay). *Under Assumption V.1 to V.3, we have the following lemma:*

$$\begin{aligned} \mathbb{E}[F(\mathbf{w}^{t+1}) - F(\mathbf{w}^t)] & \leq -\sum_{m=0}^M \left\{ \right. \\ & q_m\eta_m(1-P)\left(\frac{1}{4} - \frac{\eta_mL(B+8d_m)}{2B}\right)\mathbb{E}\|\nabla_{w_m}F(\mathbf{w}^t)\|^2 \\ & \left. + \sum_{m=0}^M q_m\eta_mL\left(\frac{1}{2} + 2\eta_mL^2\right)\mathbb{E}\|\tilde{\chi}^t - \chi^t\|^2\right\} + \mathcal{A}_1, \end{aligned} \quad (18)$$

where we denote

$$\begin{aligned} \mathcal{A}_1 = & \sum_{m=0}^M q_m\eta_m\frac{L^2}{8}\lambda^2d_m^3 + \sum_{m=0}^M q_m\eta_m^2L\left(\frac{4}{B}d_m\sigma_s^2 \right. \\ & \left. + \frac{(4-B)L^2}{4B}\lambda^2d_m^3 + \frac{2P}{B}C^2d_m + 2\sigma_{dp}^2d_m\right) + L\lambda^2d \end{aligned}$$

for the convenience of notation.

Since this analysis does not account for the effect of delayed communication, we subsequently address it in Lemma V.10. The detailed proof of these two lemmas can be found in Appendix B. We account for asynchronous device participation and bound the communication delay term $\mathbb{E}\|\tilde{\chi}^t - \chi^t\|^2$ by introducing the following Lyapunov function that captures the discrepancy between delayed and current model parameters:

$$V^t = F(\mathbf{w}^t) + \sum_{i=1}^{\tau} \gamma_i \|\chi^{t+1-i} - \chi^{t-i}\|^2 \quad (19)$$

with γ_i to be determined later.

Utilizing the Lyapunov function, we can derive Lemma V.10, which quantifies the descent of the Lyapunov function in each communication round. This lemma successfully quantifies the effect of communication delay, while the descent of Lyapunov function provides an upper bound for the descent of the objective function.

Lemma V.10. *Under Assumption V.1-V.3, and assume the device delay τ_m is uniformly upper bounded by τ , we have the following lemma:*

$$\mathbb{E}[V^{t+1} - V^t] \leq -\frac{1-P}{8}\min_m\{q_m\eta_m\}\mathbb{E}\|\nabla_{w_m}F(\mathbf{w}^t)\|^2$$

$$+ \mathcal{A}_1 + \mathcal{A}_2, \quad (20)$$

where we denote

$$\begin{aligned} \mathcal{A}_2 = & \sum_{m=1}^M q_m\eta_m^2\gamma_1\left(\frac{L^2}{4}\lambda^2d_m^3 + \frac{2}{B}d_m\sigma_s^2 + \right. \\ & \left. \frac{L^2}{2B}\lambda^2d_m^3 + \frac{P}{B}C^2d_m + \sigma_{dp}^2d_m\right) \end{aligned}$$

for the ease of notation.

By combining the descent inequality derived from Lemma V.10 with appropriate choices of step size and smoothing parameters, we obtain a bound on the average gradient norm over T iterations, which establishes the convergence rate as stated in Theorem V.4. We start from the result of Lemma V.10.

Re-arrange the terms in (20), and take average over $0, 1, \dots, T-1$:

$$\begin{aligned} & \frac{1-P}{8T}\min_m\{q_m\eta_m\}\sum_{t=0}^{T-1}\mathbb{E}\|\nabla_{w_m}F(\mathbf{w}^t)\|^2 \\ & \leq \frac{1}{T}\mathbb{E}[V^0 - V^T] + \mathcal{A}_1 + \mathcal{A}_2 \\ & \leq \frac{1}{T}\mathbb{E}[F^0 - F^T] + \mathcal{A}_1 + \mathcal{A}_2, \end{aligned}$$

where the second inequality follows from the definition of V^t in (19).

Dividing $\alpha = \frac{1}{8}\min_m\{q_m\eta_m\}$ from both sides, and plugging in \mathcal{A}_1 and \mathcal{A}_2 , we have:

$$\begin{aligned} & \frac{1-P}{T}\sum_{t=0}^{T-1}\mathbb{E}\|\nabla_{w_m}F(\mathbf{w}^t)\|^2 \\ & \leq \frac{1}{\alpha T}\mathbb{E}[F^0 - F^T] + \frac{1}{\alpha}\sum_{m=0}^M q_m\eta_m\frac{L^2}{8}\lambda^2d_m^3 \\ & \quad + \frac{1}{\alpha}\sum_{m=0}^M q_m\eta_m^2L\left(\frac{4}{B}d_m\sigma_s^2 \right. \\ & \quad \left. + \frac{(4-B)L^2}{4B}\lambda^2d_m^3 + \frac{2P}{B}C^2d_m + 2\sigma_{dp}^2d_m\right) \\ & \quad + \frac{1}{\alpha}L\lambda^2d + \frac{1}{\alpha}\sum_{m=1}^M q_m\eta_m^2\gamma_1\left(\frac{L^2}{4}\lambda^2d_m^3 + \frac{2}{B}d_m\sigma_s^2 \right. \\ & \quad \left. + \frac{L^2}{2B}\lambda^2d_m^3 + \frac{P}{B}C^2d_m + \sigma_{dp}^2d_m\right) \end{aligned}$$

For the simplicity of analysis, we let $\eta_0 = \eta_m = \eta$, $q_* = \min_m q_m$, then $\alpha = \frac{\eta}{8}q_*$. Let $d_* = \max_m d_c$, and $\lambda \leq \frac{1}{Ld\sqrt{T}}$. Thus,

$$\begin{aligned} & \frac{1-P}{T}\sum_{t=0}^{T-1}\mathbb{E}\|\nabla_{w_m}F(\mathbf{w}^t)\|^2 \\ & \leq \frac{8}{q_*\eta T}\mathbb{E}[F^0 - F^T] + \frac{2d_*^3/d^2}{q_*T} + \frac{16\eta L}{q_*}\left(\frac{4}{B}d_*\sigma_s^2 \right. \\ & \quad \left. + \frac{(4-B)d_*^3/d^2}{4BT} + \frac{2P}{B}C^2d_* + 2\sigma_{dp}^2d_*\right) \\ & \quad + \frac{8}{q_*Ld\eta T} + \frac{16\eta\gamma_1}{q_*}\left(\frac{2}{B}d_*\sigma_s^2 + \frac{(B+2)d_*^3/d^2}{4BT}\right) \end{aligned}$$

$$\begin{aligned}
& + \frac{P}{B} C^2 d_* + \sigma_{dp}^2 d_m \Big) \\
\leq & \frac{8}{q_* \eta T} \mathbb{E} [F^0 - F^T] + \frac{2d_*}{q_* T} + \frac{8}{q_* L d \eta T} \\
& + \frac{16\eta(4L + 2\gamma_1)d_*\sigma_s^2}{q_* B} + \frac{4\eta((4-B)L + (B+2)\gamma_1)d_*}{q_* B T} \\
& + \frac{16\eta(2L + \gamma_1)PC^2 d_*}{q_* B} + \frac{16\eta(2L + \gamma_1)\sigma_{dp}^2 d_*}{q_* B}
\end{aligned}$$

where in the last step, we use the fact that $d > d_*$.

If we choose $\eta = \frac{1}{\sqrt{T}d_*}$ and use Lemma V.7., we can get the convergence rate:

$$\begin{aligned}
& \frac{1}{T} \sum_{t=0}^{T-1} \mathbb{E} [\|\nabla_{\mathbf{w}} F(\mathbf{w}^t)\|^2] \\
\leq & \frac{1}{1 - \Xi} \left\{ \frac{8\sqrt{d_*}}{q_* T^{1/2}} \mathbb{E} [F^0 - F^T] + \frac{2d_*}{q_* T} + \frac{8\sqrt{d_*}}{q_* L d T^{1/2}} \right. \\
& + \frac{16(4L + 2\gamma_1)\sqrt{d_*}\sigma_s^2}{q_* B T^{1/2}} + \frac{4((4-B)L + (B+2)\gamma_1)\sqrt{d_*}}{q_* B T^{1/2}} \\
& \left. + \frac{16(2L + \gamma_1)\Xi C^2 \sqrt{d_*}}{q_* B T^{1/2}} + \frac{16(2L + \gamma_1)\sigma_{dp}^2 \sqrt{d_*}}{q_* T^{1/2}} \right\}
\end{aligned}$$

We thus conclude that the convergence rate is

$$\mathcal{O} \left(\frac{d_*^{1/2} \mathbb{E} [F^0 - F^T] + d_*^{1/2} \sigma_s^2 + d_*^{1/2} \sigma_{dp}^2}{T^{1/2}} \right),$$

where constant factors are absorbed into the $O(\cdot)$ -notation for simplicity.

VI. PRIVACY ANALYSIS

In this section, we talk about how our algorithm protects privacy under threats of label inference attacks and feature inference attacks.

A. Threat Model and Risk Evaluation

Threat Model. We consider the *honest-but-curious* (HBC) threat model, where parties correctly follow the training protocol but may attempt to infer sensitive information from exchanged messages. In particular, we assume that the server, which holds the labels and performs loss computation, is trusted, while devices, who hold partial data at local, may attempt to infer private information from intermediate results exchanged during training [37].

This assumption is motivated by typical real-world deployment scenarios of VFL, such as finance, healthcare, and online advertising, where the server corresponds to a centralized service provider (e.g., a bank, hospital, or platform operator) that owns the prediction task, maintains the training infrastructure, and is subject to strict regulatory and contractual obligations. In contrast, devices are often data holders who contribute feature sets but do not control the overall learning objective. Similar trust assumptions have been widely adopted in prior VFL works [31], [38]–[40], where attacking techniques and privacy protection is primarily designed for feature-holding parties.

Training-Time Privacy Risks in VFL. Under the HBC model, privacy risks arise from information exchanged during training. Among existing attacks, **1)** label inference attacks, which aim to recover sensitive labels by exploiting gradients or other backward information received during training, and **2)** feature inference attacks, which attempt to infer private feature values of a party, are recognized as the two dominant threats in VFL. Existing studies have shown that these two attack categories capture the primary privacy risks in VFL settings. Therefore, in this work, we focus exclusively on label inference and feature inference attacks during training.

Implications for Privacy Mechanism Design. Given this threat model, we argue that privacy protection is unnecessary for forward feature transmissions, which are sent from passive parties to the trusted server (as in VAFL [2]).

Since the server is assumed to be non-adversarial, protecting forward features does not mitigate the considered privacy risks and would unnecessarily distort the information required for accurate loss computation. In contrast, backward information, such as gradients or gradient-related signals, is transmitted from the server to potentially curious passive parties and has been shown to be the primary carrier of both label information and sensitive feature correlations. Consequently, backward messages constitute the main attack surface for both label inference and feature inference attacks under the HBC model. Therefore, we apply privacy mechanisms **exclusively to the backward information**, which effectively mitigates the dominant training-time privacy risks while preserving model utility.

B. Theoretical Differential Privacy Guarantee

In this part, we give rigorous proof for the differential privacy guarantee in Theorem VI.5.

We first introduce the definition of Gaussian differential privacy (GDP) [41] which will be useful in the proof for Theorem VI.5. Compared with traditional DP defined in (4), this notion of privacy provides a much tighter composition theorem, thus requiring less noise to be injected each round for a given privacy level.

Definition VI.1 (Gaussian Differential Privacy). Let $G_\mu := T(\mathcal{N}(0, 1), \mathcal{N}(\mu, 1))$ for $\mu \geq 0$, where the trade-off function $T(P, Q) : [0, 1] \rightarrow [0, 1]$ is defined as $T(P, Q)(\alpha) = \inf(\beta_\phi : \alpha_\phi < \alpha)$. A mechanism M is said to satisfy μ -Gaussian Differential Privacy if it satisfies

$$T(M(X), M(X')) \geq G_\mu$$

For all neighboring dataset $X, X' \in \mathcal{X}^n$.

We construct our DP algorithm based on the Gaussian Mechanism. Specifically, Gaussian mechanism ensures that, by injecting a designed Gaussian noise into a random algorithm, the algorithm is differentially private, and it provides a guidance to how large the noise should be for reaching a specific privacy level. Before presenting our results, we first present several existing results from prior works. We begin with the Gaussian mechanism under GDP, which is summarized in the following result:

Result VI.2 (Gaussian Mechanism for Gaussian Differential Privacy [41]). *Define the Gaussian mechanism that operates on a statistic θ as $M(\theta) = \theta(X) + \sigma$, where $\sigma \sim \mathcal{N}(0, r^2 C_\theta^2 / \mu^2)$, r is the sample rate for a single datum, and C_θ is the L_2 sensitivity of X . Then, M is μ -GDP.*

The repeated application of a Gaussian mechanism is known as composition. In this setting, privacy loss accumulates over iterations: adding Gaussian noise multiple times leads to a weaker aggregate privacy guarantee than a single noise injection. Accurately quantifying the resulting privacy level of iterative Gaussian mechanisms, which is exactly the scenario encountered in neural network training, necessitates the following composition theorem.

Result VI.3 (Composition of Gaussian Differential Privacy [41]). *The T -fold composition of μ -GDP mechanisms is $\sqrt{T}\mu$ -GDP*

Due to differences in their respective notational frameworks, it is not straightforward to directly compare the privacy guarantees of Gaussian DP and the conventional (ϵ, δ) -DP, which hinders fair comparison with baseline methods. To address this issue and present our results in a commonly adopted (ϵ, δ) -DP form, we leverage the following lossless conversion theorem to translate Gaussian DP guarantees into equivalent:

Result VI.4 (Conversion from Gaussian Differential Privacy to (ϵ, δ) -Differential Privacy [41]). *A mechanism is μ -GDP iff it is $(\epsilon, \delta(\epsilon))$ -DP for all $\epsilon \geq 0$, where*

$$\delta(\epsilon) = \Phi\left(-\frac{\epsilon}{\mu} + \frac{\mu}{2}\right) - e^\epsilon \Phi\left(-\frac{\epsilon}{\mu} - \frac{\mu}{2}\right) \quad (21)$$

Using the above results, we are now ready to prove the following theorem, which establishes that our algorithm is differentially private and quantifies its privacy level.

Theorem VI.5. *Under assumption V.1-V.3, suppose the privacy parameter σ_{dp} is $\sigma_{dp} = \frac{2C\sqrt{T}}{D\mu}$, where D denotes the volume of the dataset, T defines total iterations, and $\mu > 0$ controls the privacy level. The training process of Alg 1 is seen to be $(\epsilon, \delta(\epsilon))$ -differential private for $\forall \epsilon > 0$, where*

$$\delta(\epsilon) = \Phi\left(-\frac{\epsilon}{\mu} + \frac{\mu}{2}\right) - e^\epsilon \Phi\left(-\frac{\epsilon}{\mu} - \frac{\mu}{2}\right) \quad (22)$$

Proof. First recall the definition of Δ_m^t defined in (8):

$$\Delta_m^t = \frac{1}{B} \sum_{i \in \mathcal{I}_m^t} \text{clip}_C(\delta_{m,i}^{t,t_m}) + z_m^t$$

For a pair of neighboring dataset X, X' differing in only one entry of data, the L_2 sensitivity C_L of $\frac{1}{B} \sum_{i \in \mathcal{I}_m^t} \text{clip}_C(\delta_{m,i}^{t,t_m})$ follows by

$$C_L = \left\| \frac{1}{B} \sum_{i \in \mathcal{I}_m^t} \text{clip}_C(\delta_{m,i}^{t,t_m}) \right\|_2 \leq \frac{1}{B} \left\| \text{clip}_C(\delta_{m,i}^{t,t_m}) \right\|_2 \leq \frac{2C}{B}$$

The sample rate r of a single data is seen to be the batch size B divided by the size of the dataset D :

$$r = \frac{B}{D}$$

Note that in Theorem VI.5, the standard deviation of z_m^t is given by

$$\sigma_{dp} = \frac{2C\sqrt{T}}{D\mu} = \frac{(B/D)(2C/B)\sqrt{T}}{\mu} = \frac{rC_L}{(\mu/\sqrt{T})}$$

By Result VI.2, the mechanism conducted in (8) satisfies (μ/\sqrt{T}) -Gaussian Differential Privacy. Further applying the composition of GDP in Result VI.3, and by the post-processing [42] of differential privacy, we have that the whole training process of Algorithm 1 is μ -GDP. We complete the proof by converting μ -GDP to (ϵ, δ) -DP according to (21). \square

Discussion. The theorem provides privacy guarantee under the “honest-but-curious” threat model, where one or a few malicious devices try to do inference attacks by collecting information of the system. By providing only the differentially private ZO information Δ_m^t , the algorithm protects for labels [18] and per-record influence, because the attacker cannot differentiate a single datum in the dataset \mathcal{D} and label set \mathbf{Y} . The differential privacy parameter μ is related to (ϵ, δ) through the relationship defined in (22). Given any two of these parameters, the third can be determined by solving (22), allowing full flexibility in controlling the privacy level.

VII. EXPERIMENTS

A. Dataset and Baselines

We consider four datasets: image dataset MNIST [43], CIFAR-10 [44], semantic dataset Amazon Review Polarity [45], and multi-view dataset ModelNet40 [46]. For each dataset, we conduct a grid search on learning rates and other hyperparameters. We run 100 epochs on each method and select the best validation model. We run each algorithm under three random seeds and compute the sample variance for the generosity of our result. Additional information on the selection of dataset, data processing and model architecture can be found in Appendix C.

We compare our algorithm against several SotA VFL methods: 1) VAFL [2] 2) ZOO-VFL [26], 3) VFL-CZOFO [21]. All methods assume that the server holds the labels, and concatenates the embeddings of devices as the input of the server. VAFL updates its model through first-order optimization in an asynchronous manner, and achieves DP by adding random noise to the output of each local embedding. We use VAFL as a first-order baseline of VFL method. Contrary to VAFL, ZOO-VFL and VFL-CZOFO both adopt ZO optimization in their training procedure. ZOO-VFL substitutes the first order optimization by ZO optimization in common VFL methods. VFL-CZOFO uses a cascade hybrid optimization method that computes the intermediate gradient via ZOO, while keeping the back propagation on both server and device. To enforce DP and compare all methods fairly, we follow the approach in VAFL [2], applying the same DP mechanism to both VFL-CZOFO and ZOO-VFL, which involves clipping the embeddings and adding calibrated vector noise. In this paper, we only focus on the same update behavior as VAFL which updates server and device once for every communication round. In addition, model delay has been manually adjusted for all methods based on the per-batch computation time on

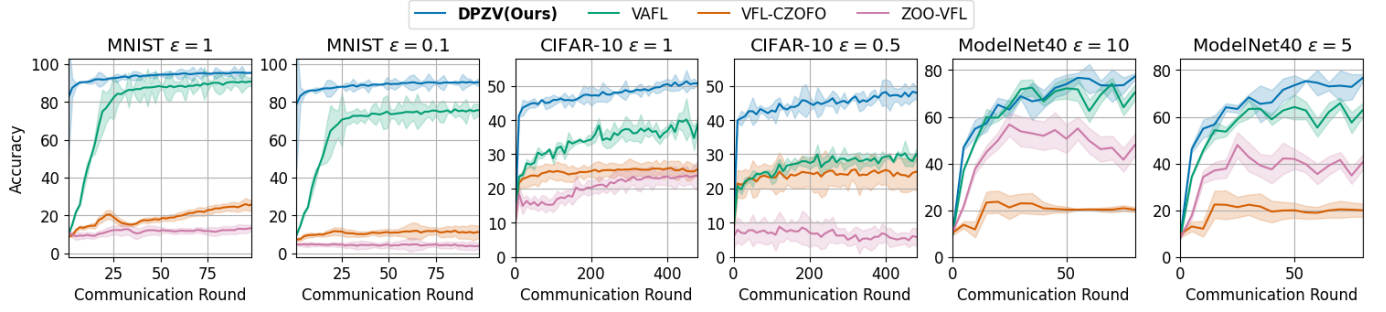


Fig. 2: Test Accuracy of VFL Methods on image classification tasks under DP constraints. δ is set to 1×10^{-3} . DPZV outperforms first-order VFL methods on two datasets and surpasses all other ZO-based methods across all three datasets, showing both a higher accuracy and a faster convergence rate.

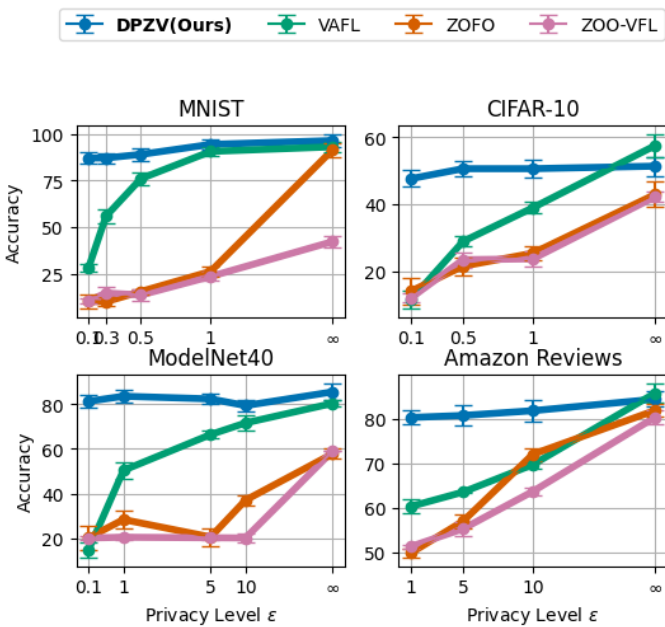


Fig. 3: Privacy-Accuracy tradeoff across different datasets and algorithms. We use a constant level of $\delta = 1 \times 10^{-3}$ and vary ϵ to simulate different privacy levels. Our algorithm consistently outperforms baselines under tight privacy budget, showing a slower decay in performance than baselines as ϵ decreases.

a single device to simulate device heterogeneity and ensure a fair comparison.

B. Analysis of Results

Accelerated convergence of DPZV with privacy guarantees. Figure 2 presents the performance evaluation of DPZV against all baselines on both image classification and language tasks under certain DP levels, where two different privacy budgets ϵ are evaluated for each dataset. On MNIST and CIFAR-10 with strict privacy constraints ($\epsilon = 1$ and $\epsilon = 0.5$, with $\delta = 1 \times 10^{-3}$), DPZV consistently achieves the highest test accuracy and faster convergence across communication rounds. As the privacy budget becomes tighter, first-order baseline VAFL exhibits a pronounced accuracy drop due to

the injection of high-dimensional noise, while the zeroth-order baseline ZOO-VFL also suffers from severe performance degradation and unstable training dynamics caused by the combined effect of zeroth-order bias and DP noise. In contrast, DPZV remains comparatively robust to increasingly stringent privacy constraints, demonstrating a significantly improved privacy-accuracy tradeoff.

On the more challenging ModelNet40 task, where training is more challenging due to larger models and a higher degree of device heterogeneity, we moderately relax the privacy budget ($\epsilon = 10$ and $\epsilon = 5$), and observe that DPZV still maintains a competitive advantage over other ZO-based methods while achieving accuracy comparable to the first-order baseline VAFL. The scalar noise injected in DPZV effectively constrains the noise magnitude, mitigating the instability typically introduced by noisy zeroth-order gradient estimators. This leads to more stable training dynamics than other ZO based methods. Moreover, in contrast to the high-dimensional vector noise used in first-order baseline VAFL, scalar noise incurs significantly less optimization distortion, enabling DPZV to achieve a more favorable privacy-accuracy tradeoff and, consequently, fewer communication rounds to reach a target accuracy.

DPZV elevates privacy-utility tradeoff. Figure 3 presents the accuracy-privacy tradeoff across four benchmark datasets: MNIST, CIFAR-10, ModelNet40, and Amazon Reviews. We evaluate the robustness of our proposed method DPZV under various privacy budgets ϵ , while fixing the failure probability $\delta = 1 \times 10^{-3}$. Across all tasks, DPZV consistently achieves the highest accuracy under tight privacy regimes ($\epsilon \leq 1$), indicating its ability to maintain model utility even with stringent differential privacy constraints. Notably, on MNIST and ModelNet40, DPZV shows only a marginal drop in accuracy as ϵ decreases, while the competing methods suffer substantial degradation. For instance, on CIFAR-10 at $\epsilon = 0.1$, DPZV maintains over 90% accuracy, whereas VFL-CZOFO and ZOO-VFL fall below 30%. Similar trends are observed on Amazon Reviews, where DPZV consistently outperforms baselines under strict privacy, especially at $\epsilon = 1$ and $\epsilon = 5$. These results validate the effectiveness of our scalar-noise-based DP mechanism in balancing utility and privacy, and highlight its advantage in real-world privacy-sensitive federated learning

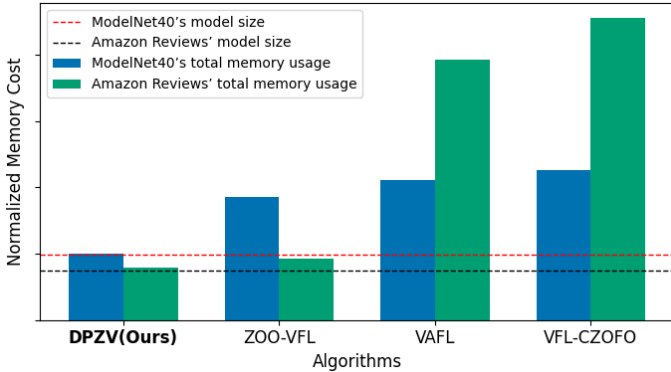


Fig. 4: Normalized memory cost in training for each method. DPZV requires the smallest memory allocation in both datasets, almost the same as model memory itself. This shows the memory efficiency of DPZV, allowing superior performance on large-scale neural networks.

TABLE I: Total communication cost incurred by each method until reaching a fixed target accuracy for each dataset. The target accuracy for each dataset is 90%, 40%, 50%, and 80%

Dataset	DPZV(Ours)	VAFL	CZOfirst-order	ZOO-VFL
MNIST(MB)	576.0 \pm 31.7	1209.6 \pm 98.9	4492.8 \pm 261.7	∞
CIFAR-10(GB)	2.74 \pm 0.16	2.26 \pm 0.12	20.02 \pm 1.94	23.90 \pm 3.25
ModelNet40(MB)	302.4 \pm 17.7	423.36 \pm 22.0	604.8 \pm 28.2	5927.04 \pm 328.5
Amazon Reviews(GB)	13.27 \pm 0.78	16.59 \pm 0.86	36.59 \pm 3.70	69.67 \pm 3.86

scenarios.

DPZV mitigates memory overhead. Figure 4 compares the GPU memory consumption, with memory values normalized for readability. We compare the memory cost on larger models, where we use ResNet for image classification and BERT for sequence classification. We record the highest memory peak to show the total required memory for each method on training large models. We observe that DPZV requires memory approximately equal to the model size, whereas the first-order method VAFL demands more than twice the model size. Compared to ZOO-VFL, DPZV achieves further memory savings by leveraging MeZO. *These results highlight the scalability of DPZV, making it well-suited for deploying large pretrained language models in VFL scenarios.*

C. Communication Efficiency Evaluation

We quantify the communication volume of the network by

$$\mathcal{V}_T = \sum_{t=1}^T \sum_{m=1}^M (N_{t,m}^{\text{up}} + N_{t,m}^{\text{down}}), \quad (23)$$

where $N_{t,m}^{\text{up}}$ and $N_{t,m}^{\text{down}}$ denote the sizes (in bytes) of the tensors transmitted in the uplink and downlink, respectively, between the server and device m at communication round t . This metric measures the total communication cost as the cumulative number of bytes exchanged over all devices and rounds.

Evaluation on Total Communication Cost. Table I reports the total communication cost \mathcal{V}_T required to reach a target accuracy, which is set to be 90%, 40%, 50%, and 80% for each dataset, respectively. The metric (23) captures the end-to-end

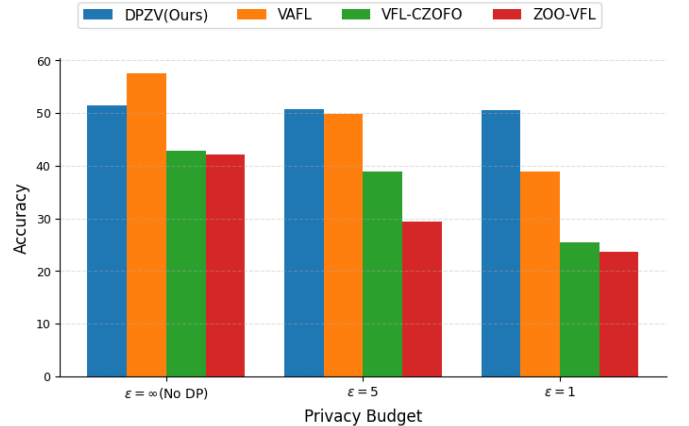


Fig. 5: Achieved accuracy under fixed communication cost on CIFAR-10 under different privacy budget. δ is set to 1×10^{-3} .

communication cost over the entire training process, reflecting both convergence speed and stability under differential privacy constraints.

Across the evaluated datasets, DPZV consistently achieves low total communication cost and often outperforms both first-order and ZO baselines. In particular, DPZV significantly reduces communication cost compared to existing ZO methods, while remaining competitive with the first-order baseline VAFL. In contrast, ZO baselines such as VFL-CZOFO and ZOO-VFL incur substantially higher transmitted bytes, and in some cases fail to reach the target accuracy within the training budget. These results underscore the importance of an improved privacy–accuracy tradeoff, as poor convergence under privacy constraints directly translates into excessive communication overhead. By converging in fewer rounds under privacy constraints, DPZV reduces the total communication cost required to attain a desired accuracy.

Communication Efficiency under Differential Privacy Budget. Figure 5 evaluates model accuracy under a fixed total communication budget, highlighting how differential privacy alters the effectiveness of each transmitted byte. In the non-private setting ($\epsilon = \infty$), the first-order baseline VAFL achieves the highest accuracy, which is consistent with standard optimization theory: in the absence of privacy constraints, first-order methods benefit from exact gradient information and therefore typically outperform ZO alternatives. In contrast, ZO methods, including DPZV, rely on gradient estimation from function evaluations and may incur a modest performance gap when no privacy noise is present.

However, this advantage of VAFL diminishes rapidly as privacy constraints are introduced. As the privacy budget decreases to $\epsilon = 5$ and further to $\epsilon = 1$, VAFL experiences a substantial accuracy drop, despite transmitting the same number of bytes. This is because enforcing differential privacy requires injecting high-dimensional noise into gradient updates, causing a large fraction of communicated information to be dominated by noise rather than optimization signal. The degradation is even more pronounced for ZO baselines such as ZOO-VFL. While VFL-CZOFO exhibits improved

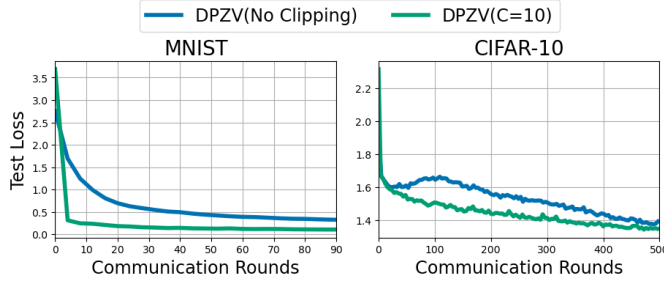


Fig. 6: Effect of gradient clipping on DPZV under non-private settings. We compare models trained with and without clipping of the ZO information. Across both MNIST and CIFAR-10, clipping accelerates convergence and stabilizes training.

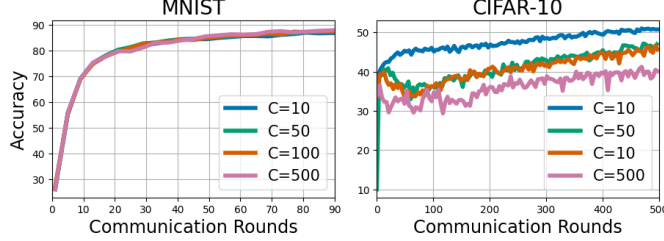


Fig. 7: Effect of clipping threshold on DPZV under differential privacy constraint $\epsilon = 1$. While all clipping levels perform similarly on MNIST, smaller thresholds ($C = 10$) significantly improve accuracy and convergence on CIFAR-10.

robustness relative to ZOO-VFL, it still incurs significant performance loss under tight privacy budgets. In contrast, DPZV maintains consistently strong performance across all privacy regimes, with only marginal degradation as the privacy budget tightens. By injecting scalar noise rather than high-dimensional vector noise, DPZV effectively limits variance amplification. As a result, DPZV achieves a markedly superior privacy–communication–accuracy tradeoff, enabling more effective utilization of the communication budget and requiring fewer rounds to reach a target accuracy under strict privacy constraints. From a communication perspective, DPZV preserves a higher signal-to-noise ratio per transmission, enabling faster accuracy recovery under the same communication budget.

D. Ablation Study

Clipping benefits convergence. We observe in Figure 3 that even under no privacy constraints ($\epsilon = \infty$), DPZV outperforms other ZO based algorithms. A key distinction lies in DPZV’s use of scalar clipping on ZO information, while originally introduced for differential privacy, also acts as a form of gradient regularization. This regularization effect has been shown to improve convergence in prior work [47], and we observe similar benefits here. Figure 6 verifies our insight by comparing the convergence behavior of DPZV with and without gradient clipping under a non-private setting. The plots show test loss versus communication rounds. In both datasets, applying clipping to the ZO information significantly improves convergence speed. For MNIST, clipped DPZV reaches low test loss much faster and stabilizes more smoothly. On CIFAR-10, the clipped version also demonstrates consistently lower

loss throughout training. These results suggest that clipping not only stabilizes training but also enhances convergence efficiency, even when privacy is not enforced.

Impact of Sensitivity Level. Figure 7 presents the performance of DPZV under different sensitivity levels, which is controlled by the clipping threshold C . We apply a fixed privacy budget of $\epsilon = 1, \delta = 1 \times 10^{-3}$ on both MNIST and CIFAR-10. In the MNIST setting, all clipping levels achieve similar convergence and final accuracy, suggesting the model is robust to the choice of C in simple tasks. In contrast, the CIFAR-10 results highlight a pronounced impact: smaller clipping values (e.g., $C = 10$) yield better accuracy and stability over training. Larger thresholds, such as $C = 500$ degrade performance, likely due to the excessive noise required to satisfy DP constraints. These results emphasize the importance of careful clipping calibration in more complex settings to ensure a good privacy-utility tradeoff.

VIII. CONCLUSION AND FUTURE WORK

In this paper, we proposed DPZV, a differentially private zeroth-order vertical federated learning framework designed for privacy-critical and bandwidth-constrained settings. By eliminating explicit gradient transmission and injecting calibrated scalar noise at the server, DPZV achieves tunable (ϵ, δ) -differential privacy while avoiding the variance amplification associated with high-dimensional noise in existing VFL methods, thereby mitigating key privacy risks such as label inference. We established convergence guarantees under asynchronous updates and bounded delays, highlighting an underexplored advantage of zeroth-order optimization for private federated learning. Extensive experiments on image and language tasks demonstrate that DPZV consistently outperforms both first-order and zeroth-order VFL baselines across a wide range of privacy budgets, achieving improved accuracy, stability, and scalability under strict privacy constraints.

Future work includes extending DPZV to stronger adversarial models and adaptive privacy mechanisms, broadening the applicability of zeroth-order methods in privacy-preserving collaborative learning.

REFERENCES

- [1] S. Hardy, W. Henecka, H. Ivey-Law, R. Nock, G. Patrini, G. Smith, and B. Thorne, “Private federated learning on vertically partitioned data via entity resolution and additively homomorphic encryption,” *arXiv preprint arXiv:1711.10677*, 2017.
- [2] T. Chen, X. Jin, Y. Sun, and W. Yin, “Vafl: a method of vertical asynchronous federated learning,” *arXiv preprint arXiv:2007.06081*, 2020.
- [3] T. Castiglia, S. Wang, and S. Patterson, “Flexible vertical federated learning with heterogeneous parties,” *IEEE Transactions on Neural Networks and Learning Systems*, 2023.
- [4] S. Wang, T. Tuor, T. Salonidis, K. K. Leung, C. Makaya, T. He, and K. Chan, “When edge meets learning: Adaptive control for resource-constrained distributed machine learning,” in *IEEE INFOCOM 2018-IEEE conference on computer communications*. IEEE, 2018, pp. 63–71.
- [5] W. Shi, J. Cao, Q. Zhang, Y. Li, and L. Xu, “Edge computing: Vision and challenges,” *IEEE internet of things journal*, vol. 3, no. 5, pp. 637–646, 2016.
- [6] J. Park, S. Samarakoon, M. Bennis, and M. Debbah, “Wireless network intelligence at the edge,” *Proceedings of the IEEE*, vol. 107, no. 11, pp. 2204–2239, 2019.

[7] J. Guo, R. G. Raj, D. J. Love, and C. G. Brinton, "Nonparametric decentralized detection and sparse sensor selection via multi-sensor online kernel scalar quantization," *IEEE Transactions on Signal Processing*, vol. 70, pp. 2593–2608, 2022.

[8] D. Yu, W. Li, H. Xu, and L. Zhang, "Low reliable and low latency communications for mission critical distributed industrial internet of things," *IEEE Communications Letters*, vol. 25, no. 1, pp. 313–317, 2020.

[9] Y. Liu, Y. Kang, T. Zou, Y. Pu, Y. He, X. Ye, Y. Ouyang, Y.-Q. Zhang, and Q. Yang, "Vertical federated learning: Concepts, advances, and challenges," *IEEE Transactions on Knowledge and Data Engineering*, 2024.

[10] Y. Liu, Z. Yi, and T. Chen, "Backdoor attacks and defenses in feature-partitioned collaborative learning," *arXiv preprint arXiv:2007.03608*, 2020.

[11] H. Weng, J. Zhang, X. Ma, F. Xue, T. Wei, S. Ji, and Z. Zong, "Practical privacy attacks on vertical federated learning," *arXiv preprint arXiv:2011.09290*, 2020.

[12] B. McMahan, E. Moore, D. Ramage, S. Hampson, and B. A. y Arcas, "Communication-efficient learning of deep networks from decentralized data," in *Artificial intelligence and statistics*. PMLR, 2017, pp. 1273–1282.

[13] Z. Qin, G. Y. Li, and H. Ye, "Federated learning and wireless communications," *Wireless Commun.*, vol. 28, no. 5, p. 134–140, Oct. 2021. [Online]. Available: <https://doi.org/10.1109/MWC.011.2000501>

[14] J. So, B. Güler, and A. S. Avestimehr, "Byzantine-resilient secure federated learning," *IEEE Journal on Selected Areas in Communications*, vol. 39, no. 7, pp. 2168–2181, 2021.

[15] T. Castiglia, Y. Zhou, S. Wang, S. Kadhe, N. Baracaldo, and S. Patterson, "Less-vfl: Communication-efficient feature selection for vertical federated learning," in *International Conference on Machine Learning*. PMLR, 2023, pp. 3757–3781.

[16] X. Jin, P.-Y. Chen, C.-Y. Hsu, C.-M. Yu, and T. Chen, "Cafe: Catastrophic data leakage in vertical federated learning," *Advances in Neural Information Processing Systems*, vol. 34, pp. 994–1006, 2021.

[17] P. Ye, Z. Jiang, W. Wang, B. Li, and B. Li, "Feature reconstruction attacks and countermeasures of dnn training in vertical federated learning," *IEEE Transactions on Dependable and Secure Computing*, 2024.

[18] C. Fu, X. Zhang, S. Ji, J. Chen, J. Wu, S. Guo, J. Zhou, A. X. Liu, and T. Wang, "Label inference attacks against vertical federated learning," in *31st USENIX security symposium (USENIX Security 22)*, 2022, pp. 1397–1414.

[19] T. Zou, Y. Liu, Y. Kang, W. Liu, Y. He, Z. Yi, Q. Yang, and Y.-Q. Zhang, "Defending batch-level label inference and replacement attacks in vertical federated learning," *IEEE Transactions on Big Data*, 2022.

[20] S. Lee, W. Fang, A. B. Das, S. Hosseinalipour, D. J. Love, and C. G. Brinton, "Cooperative decentralized backdoor attacks on vertical federated learning," *IEEE Transactions on Networking*, 2025.

[21] G. Wang, B. Gu, Q. Zhang, X. Li, B. Wang, and C. X. Ling, "A unified solution for privacy and communication efficiency in vertical federated learning," *Advances in Neural Information Processing Systems*, vol. 36, 2024.

[22] C. Xie, P.-Y. Chen, Q. Li, A. Nourian, C. Zhang, and B. Li, "Improving privacy-preserving vertical federated learning by efficient communication with admm," in *2024 IEEE Conference on Secure and Trustworthy Machine Learning (SaTML)*. IEEE, 2024, pp. 443–471.

[23] R. Xu, N. Baracaldo, Y. Zhou, A. Anwar, and H. Ludwig, "Hybridalpha: An efficient approach for privacy-preserving federated learning," in *Proceedings of the 12th ACM workshop on artificial intelligence and security*, 2019, pp. 13–23.

[24] Y. Nesterov and V. Spokoiny, "Random gradient-free minimization of convex functions," *Foundations of Computational Mathematics*, vol. 17, no. 2, pp. 527–566, 2017.

[25] W. Fang, Z. Yu, Y. Jiang, Y. Shi, C. N. Jones, and Y. Zhou, "Communication-efficient stochastic zeroth-order optimization for federated learning," *IEEE Transactions on Signal Processing*, vol. 70, pp. 5058–5073, 2022.

[26] Q. Zhang, B. Gu, Z. Dang, C. Deng, and H. Huang, "Desirable companion for vertical federated learning: New zeroth-order gradient based algorithm," in *Proceedings of the 30th ACM International Conference on Information & Knowledge Management*, 2021, pp. 2598–2607.

[27] D. Gupta, M. Razaviyayn, and V. Sharan, "On the inherent privacy of two point zeroth order projected gradient descent," in *OPT 2024: Optimization for Machine Learning*, 2024.

[28] S. Ghadimi and G. Lan, "Stochastic first-and zeroth-order methods for nonconvex stochastic programming," *SIAM journal on optimization*, vol. 23, no. 4, pp. 2341–2368, 2013.

[29] Y. Liu, X. Zhang, Y. Kang, L. Li, T. Chen, M. Hong, and Q. Yang, "Fedbcd: A communication-efficient collaborative learning framework for distributed features," *IEEE Transactions on Signal Processing*, vol. 70, pp. 4277–4290, 2022.

[30] Y. Hu, D. Niu, J. Yang, and S. Zhou, "Fdml: A collaborative machine learning framework for distributed features," in *Proceedings of the 25th ACM SIGKDD International Conference on Knowledge Discovery & Data Mining*, 2019, pp. 2232–2240.

[31] K. Cheng, T. Fan, Y. Jin, Y. Liu, T. Chen, D. Papadopoulos, and Q. Yang, "Secureboost: A lossless federated learning framework," *IEEE intelligent systems*, vol. 36, no. 6, pp. 87–98, 2021.

[32] S. Malladi, T. Gao, E. Nichani, A. Damian, J. D. Lee, D. Chen, and S. Arora, "Fine-tuning language models with just forward passes," *Advances in Neural Information Processing Systems*, vol. 36, pp. 53 038–53 075, 2023.

[33] L. Zhang, B. Li, K. K. Thekumparampil, S. Oh, and N. He, "Dpzero: Private fine-tuning of language models without backpropagation," in *Forty-first International Conference on Machine Learning*, 2024.

[34] X. Tang, A. Panda, M. Nasr, S. Mahloujifar, and P. Mittal, "Private fine-tuning of large language models with zeroth-order optimization," *arXiv preprint arXiv:2401.04343*, 2024.

[35] O. Shamir, "An optimal algorithm for bandit and zero-order convex optimization with two-point feedback," *Journal of Machine Learning Research*, vol. 18, no. 52, pp. 1–11, 2017.

[36] X. Chen, S. Z. Wu, and M. Hong, "Understanding gradient clipping in private sgd: A geometric perspective," *Advances in Neural Information Processing Systems*, vol. 33, pp. 13 773–13 782, 2020.

[37] N. Papernot, P. McDaniel, A. Sinha, and M. P. Wellman, "Sok: Security and privacy in machine learning," in *2018 IEEE European symposium on security and privacy (EuroS&P)*. IEEE, 2018, pp. 399–414.

[38] Y. Wu, S. Cai, X. Xiao, G. Chen, and B. C. Ooi, "Privacy preserving vertical federated learning for tree-based models," *arXiv preprint arXiv:2008.06170*, 2020.

[39] R. Xu, N. Baracaldo, Y. Zhou, A. Anwar, J. Joshi, and H. Ludwig, "Fedv: Privacy-preserving federated learning over vertically partitioned data," in *Proceedings of the 14th ACM workshop on artificial intelligence and security*, 2021, pp. 181–192.

[40] M. Ye, W. Shen, B. Du, E. Snelzko, V. Kovalev, and P. C. Yuen, "Vertical federated learning for effectiveness, security, applicability: A survey," *ACM Computing Surveys*, vol. 57, no. 9, pp. 1–32, 2025.

[41] J. Dong, A. Roth, and W. J. Su, "Gaussian differential privacy," *Journal of the Royal Statistical Society: Series B (Statistical Methodology)*, vol. 84, no. 1, pp. 3–37, 2022.

[42] C. Dwork, A. Roth *et al.*, "The algorithmic foundations of differential privacy," *Foundations and Trends® in Theoretical Computer Science*, vol. 9, no. 3–4, pp. 211–407, 2014.

[43] L. Deng, "The mnist database of handwritten digit images for machine learning research [best of the web]," *IEEE signal processing magazine*, vol. 29, no. 6, pp. 141–142, 2012.

[44] A. Krizhevsky, G. Hinton *et al.*, "Learning multiple layers of features from tiny images," 2009.

[45] J. McAuley and J. Leskovec, "Hidden factors and hidden topics: understanding rating dimensions with review text," in *Proceedings of the 7th ACM conference on Recommender systems*, 2013, pp. 165–172.

[46] Z. Wu, S. Song, A. Khosla, F. Yu, L. Zhang, X. Tang, and J. Xiao, "3d shapenets: A deep representation for volumetric shapes," in *Proceedings of the IEEE conference on computer vision and pattern recognition*, 2015, pp. 1912–1920.

[47] J. Zhang, T. He, S. Sra, and A. Jadbabaie, "Why gradient clipping accelerates training: A theoretical justification for adaptivity," *arXiv preprint arXiv:1905.11881*, 2019.

[48] J. Devlin, "Bert: Pre-training of deep bidirectional transformers for language understanding," *arXiv preprint arXiv:1810.04805*, 2018.

APPENDIX

A. Preliminaries and Outline

We first define the following notation table to facilitate the proof:

Notation	Description
$\mathbf{w} = [w_0, w_1, w_2, \dots, w_M]$	All learnable parameters
d_0, d_1, \dots, d_M	Dimension of parameters on server (machine 0) and device $1, \dots, M$
$d = \sum_{m=0}^M d_m$	Dimension of all parameters
$f(\mathbf{w}; \xi_i) := \mathcal{L}(w_0, h_{1,i}, h_{2,i}, \dots, h_{M,i}; y_i)$	Loss function with regard to datum with ID i
$F(\mathbf{w}) := F(\mathbf{w}; \mathcal{D}, \mathbf{Y})$	Global loss function
$\chi^t = [w_1^{t_1}, \dots, w_M^{t_M}]$	Latest learnable parameters of all devices at server time t
$\tilde{\chi}^t = [w_1^{t_1 - \tau_1^t}, \dots, w_M^{t_M - \tau_M^t}]$	Delayed learnable parameters of all devices at server time t
$\mathbf{w}^t = [w_0^t, w_1^{t_1}, \dots, w_M^{t_M}]$	Latest learnable parameters of all devices and the server at server time t
$\tilde{\mathbf{w}}^t = [w_0^{t - \tau_1^t}, w_1^{t_1 - \tau_1^t}, \dots, w_M^{t_M - \tau_M^t}]$	Delayed learnable parameters of all devices and the server at server time t
$h_{m,i}^{t_m \pm} = h_m(w_m^{t_m} \pm \lambda_m \mathbf{u}_m^{t_m}; \xi_m, i)$	Local embeddings of device m for data sample i at device time t_m under the perturbed parameters
$\delta_{m,i}^{t,t_m}$ as defined in (7)	zeroth-order difference information from device m and data sample i at server time t and device time t_m
$g_{m,i}^t(\tilde{\mathbf{w}}^t) = \delta_{m,i}^{t,t_m} \mathbf{u}_m^{t_m}$	zeroth-order gradient estimator from device m and data sample i at server time t (with delay)
$\check{g}_{m,i}^t(\tilde{\mathbf{w}}^t) = \text{clip}_C(\delta_{m,i}^{t,t_m}) \mathbf{u}_m^{t_m}$	Clipped zeroth-order gradient estimator from device m and data sample i at server time t (with delay)
$\check{G}_m^t(\tilde{\mathbf{w}}^t) = (1/B) \sum_{i \in \mathcal{I}_m^{t_m}} \check{g}_{m,i}^t(\tilde{\mathbf{w}}^t) + z_m^{t_m} \mathbf{u}_m^{t_m}$	Clipped differential private zeroth-order gradient estimator from device m at server time t (with delay)
$G_m^t(\tilde{\mathbf{w}}^t) = (1/B) \sum_{i \in \mathcal{I}_m^{t_m}} g_{m,i}^t(\tilde{\mathbf{w}}^t) + z_m^{t_m} \mathbf{u}_m^{t_m}$	Non-clipped differential private zeroth-order gradient estimator from device m at server time t (with delay)

TABLE II: Table of Notations

Note that in the notation table, we use “ $\check{\cdot}$ ” to define clipped gradient estimators, and we use “ $\tilde{\cdot}$ ” to denote delayed model parameters. In the rest of the proof, we also use gradient estimators parameterized by the no delaying parameters \mathbf{w} instead of $\tilde{\mathbf{w}}$ to assume that we update the model without delay. To begin with, we restate the assumptions required for establishing the convergence analysis.

Assumption A.1 (ℓ -Lipschitz). The function $f(\mathbf{w}; \xi)$ is ℓ -Lipschitz continuous for every ξ .

Assumption A.2 (L -Smooth). The function $f(\mathbf{w}; \xi)$ is L -Smooth for every ξ . Specifically, there exists an $L > 0$ for all $m = 0, \dots, M$ such that $\|\nabla_{w_m} f(\mathbf{w}) - \nabla_{w_m} f(\mathbf{w}')\| \leq L \|\mathbf{w} - \mathbf{w}'\|$.

Assumption A.3 (Bounded gradient variance). The variance of the stochastic first order gradient is upper bounded in expectation:

$$\mathbb{E} \left[\|\nabla_{\mathbf{w}} f(\mathbf{w}; \xi) - \nabla_{\mathbf{w}} F(\mathbf{w})\|^2 \right] \leq \sigma_s^2$$

Assumption A.4 (Independent Participation). The probability of one device participating in one communication round is independent of other devices and satisfies

$$\mathbb{P}(\text{device } m \text{ uploading}) = q_m$$

Specially, we set $q_0 = 1$ as the server always participates in the update.

One of the important parts in the proof of Theorem V.4 is to bound the zeroth-order gradient estimator. We first introduce the formal definition of zeroth-order two-point gradient estimator that is used in our algorithm, and prove some technical lemmas that reveal some important properties.

Definition A.5. Let \mathbf{u} be uniformly sampled from the Euclidean sphere $\sqrt{d}\mathbb{S}^{d-1}$. For any function $f(x) : \mathbb{R}^d \rightarrow \mathbb{R}$ and $\lambda > 0$, we define its zeroth-order gradient estimator as

$$g(\mathbf{w}) = \frac{(f(\mathbf{w} + \lambda \mathbf{u}) - f(\mathbf{w} - \lambda \mathbf{u}))}{2\lambda} \mathbf{u} \quad (24)$$

Lemma A.6 (Restatement of Lemma V.6). *Let $g(\mathbf{w})$ be the zeroth-order gradient estimator defined as in (24), with $f(\mathbf{w})$ being the loss function. We define the smoothed function $f_{\lambda}(\mathbf{w}) = \mathbb{E}_{\mathbf{u}}[f(\mathbf{w} + \lambda \mathbf{u})]$, where \mathbf{u} is uniformly sampled from the Euclidean ball $\sqrt{d}\mathbb{B}^d = \{\mathbf{w} \in \mathbb{R}^d \mid \|\mathbf{w}\| \leq \sqrt{d}\}$. The following properties hold:*

- (i) $f_{\lambda}(\mathbf{w})$ is differentiable and $\mathbb{E}_{\mathbf{u}}[g(\mathbf{w})] = \nabla f_{\lambda}(\mathbf{w})$.

(ii) If $f(\mathbf{w})$ is L -smooth, we have that

$$\|\nabla f(\mathbf{w}) - \nabla f_\lambda(\mathbf{w})\| \leq \frac{L}{2} \lambda d^{3/2}, \quad (25)$$

$$|f(\mathbf{w}) - f_\lambda(\mathbf{w})| \leq \frac{L}{2} \lambda^2 d, \quad (26)$$

and

$$\mathbb{E}_{\mathbf{u}}[\|g_\lambda(\mathbf{w})\|^2] \leq 2d \cdot \|\nabla f(\mathbf{w})\|^2 + \frac{L^2}{2} \lambda^2 d^3. \quad (27)$$

Based on (14), we can further show:

$$\|\nabla f_\lambda(\mathbf{w})\|^2 \leq 2\|\nabla f(\mathbf{w})\|^2 + \frac{L^2}{2} \lambda^2 d^3 \quad (28)$$

$$\|\nabla f(\mathbf{w})\|^2 \leq 2\|\nabla f_\lambda(\mathbf{w})\|^2 + \frac{L^2}{2} \lambda^2 d^3 \quad (29)$$

This is the standard result of zeroth-order optimization. The proof of the Lemma is given by [24]. We also find the following lemmas useful in the proof:

Lemma A.7. Let \mathbf{u} be uniformly sampled from the Euclidean sphere $\sqrt{d}S^{d-1}$, and \mathbf{a} be any vector of constant value. We have that $\mathbb{E}[\mathbf{u}] = 0$ and

$$\mathbb{P}(|\mathbf{u}^\top \mathbf{a}| \geq C) \leq 2\sqrt{2\pi} \exp\left(-\frac{C^2}{8\|\mathbf{a}\|^2}\right).$$

Proof. This lemma follows exactly from Lemma C.1. in [33]. \square

Lemma A.8 (Restatement of Lemma V.7). Let Q be the event that clipping happened for a sample ξ , d be the model dimension, and L, ℓ be the Lipschitz and smooth constant as defined in assumption A.1 and assumption A.2. For $\forall C_0 > 0$, if the clipping threshold C follows $C \geq C_0 + L\lambda d/2$, we have the following upper bound for the probability of clipping:

$$P = \mathbb{P}(Q) \leq 2\sqrt{2\pi} \exp\left(-\frac{C_0^2}{8\ell^2}\right) = \Xi \quad (30)$$

Proof. Since $f(\mathbf{u}; \xi)$ is L -Smooth for every ξ , we have

$$\begin{aligned} \frac{|f(\mathbf{w} + \lambda\mathbf{u}; \xi) - f(\mathbf{w} - \lambda\mathbf{u}; \xi)|}{2\lambda} &\leq |\mathbf{u}^\top \nabla f(\mathbf{u}; \xi)| + \frac{|f(\mathbf{w} + \lambda\mathbf{u}; \xi) - f(\mathbf{w}; \xi) - \lambda\mathbf{u}^\top \nabla f(\mathbf{w}; \xi)|}{2\lambda} \\ &\quad + \frac{|f(\mathbf{w} - \lambda\mathbf{u}; \xi) - f(\mathbf{w}; \xi) + \lambda\mathbf{u}^\top \nabla f(\mathbf{w}; \xi)|}{2\lambda} \\ &\leq |\mathbf{u}^\top \nabla f(\mathbf{w}; \xi)| + \frac{L}{2}\lambda. \end{aligned}$$

Therefore, by Lemma A.7 and Assumption A.1, we obtain

$$\begin{aligned} \mathbb{P}(Q) &= \mathbb{P}\left(\frac{|f(\mathbf{w} + \lambda\mathbf{u}; \xi_i) - f(\mathbf{w} - \lambda\mathbf{u}; \xi_i)|}{2\lambda} \geq C_0 + \frac{L}{2}\lambda\right) \\ &\leq \mathbb{P}(|\mathbf{u}^\top \nabla f(\mathbf{w}; \xi_i)| \geq C_0) \\ &\leq 2\sqrt{2\pi} \exp\left(-\frac{C_0^2}{8\|\nabla f(\mathbf{w}; \xi_i)\|^2}\right) \\ &\leq 2\sqrt{2\pi} \exp\left(-\frac{C_0^2}{8\ell^2}\right). \end{aligned}$$

\square

Lemma A.9 (Expectation and Variance of Clipped Zeroth-order Gradient Estimator). Recall that $\check{g}_{m,i}^t(\mathbf{w}^t)$ is defined as the clipped zeroth-order gradient estimator assuming no communication delay, random perturbation \mathbf{u} is defined in Lemma A.7, and event Q is defined in Lemma V.7. We have the following properties:

(i) When taking expectation w.r.t \mathbf{u} and Q , the clipped zeroth-order gradient estimator follows

$$\mathbb{E}_{\mathbf{u}}[\check{g}_{m,i}^t(\mathbf{w}^t)] = (1 - P)\nabla_{w_m} F_\lambda(\mathbf{w}^t) \quad (31)$$

(ii) The variance of $\check{g}_{m,i}^t(\mathbf{w}^t)$ follows

$$\text{Var}(\check{g}_{m,i}^t(\mathbf{w}^t)) \leq (1-P)(2d_m\|\nabla_{w_m}F(\mathbf{w}^t)\|^2 + 2d_m\sigma_s^2 + \frac{L^2}{2}\lambda^2d_m^3) + PC^2d_m - (1-P)^2\|\nabla_{w_m}F_\lambda(\mathbf{w}^t)\|^2 \quad (32)$$

Proof. For (i), we have

$$\begin{aligned} \mathbb{E}[\check{g}_{m,i}^t(\mathbf{w}^t)] &= \mathbb{E}[\check{g}_{m,i}^t(\mathbf{w}^t)|\bar{Q}]\mathbb{P}(\bar{Q}) + \mathbb{E}[\check{g}_{m,i}^t(\mathbf{w}^t)|Q]\mathbb{P}(Q) \\ &= \mathbb{E}[\check{g}_{m,i}^t(\mathbf{w}^t)](1-\mathbb{P}(Q)) + \mathbb{E}[C\mathbf{u}_m^t]\mathbb{P}(Q) \\ &= (1-P)\nabla_{w_m}F_\lambda(\mathbf{w}^t) \end{aligned}$$

where in the first step we applied the Law of Total Expectation, and in the last step we used the property (i) in Lemma V.6 and (i) in Lemma A.7.

By (31), we can further bound the variance of $\check{g}_{m,i}^t$,

$$\begin{aligned} \text{Var}(\check{g}_{m,i}^t(\mathbf{w}^t)) &= \mathbb{E}\left[\left\|\check{g}_{m,i}^t(\mathbf{w}^t) - (1-P)\nabla_{w_m}F_\lambda(\mathbf{w}^t)\right\|^2\right] \\ &= \mathbb{E}\left[\left\|\check{g}_{m,i}^t(\mathbf{w}^t)\right\|^2\right] - (1-P)^2\|\nabla_{w_m}F_\lambda(\mathbf{w}^t)\|^2 \\ &= \mathbb{E}\left[\left\|\check{g}_{m,i}^t(\mathbf{w}^t)\right\|^2|\bar{Q}\right]\mathbb{P}(\bar{Q}) + \mathbb{E}\left[C^2\|\mathbf{u}_m^t\|^2|Q\right]\mathbb{P}(Q) - (1-P)^2\|\nabla_{w_m}F_\lambda(\mathbf{w}^t)\|^2 \\ &\stackrel{1)}{\leq} (1-P)(2d_m\|\nabla_{w_m}f(\mathbf{w}^t; \xi_{m,t})\|^2 + \frac{L^2}{2}\lambda^2d_m^3) \\ &\quad + PC^2d_m - (1-P)^2\|\nabla_{w_m}F_\lambda(\mathbf{w}^t)\|^2 \\ &\stackrel{2)}{\leq} (1-P)(2d_m\|\nabla_{w_m}F(\mathbf{w}^t)\|^2 + 2d_m\sigma_s^2 + \frac{L^2}{2}\lambda^2d_m^3) \\ &\quad + PC^2d_m - (1-P)^2\|\nabla_{w_m}F_\lambda(\mathbf{w}^t)\|^2 \end{aligned}$$

where 1) is by the property of zeroth-order gradient estimator (15) and 2) follows from the bounded gradient assumption (Assumption A.3). \square

Lemma A.10 (Restatement of Lemma V.8). *Let $\check{G}_m^t(\mathbf{w}^t)$ be the Differential Private Zeroth-order Gradient without delay. Under the same condition as Lemma V.6, we can bound the variance of $\check{G}_m^t(\mathbf{w}^t)$ in expectation, with the expectation taken on random direction \mathbf{u} , DP noise z , and clipping event Q :*

$$\begin{aligned} \text{Var}(\check{G}_m^t(\mathbf{w}^t)) &\leq \frac{1-P}{B}(2d_m\mathbb{E}\left[\|\nabla_{w_m}F(\mathbf{w}^t)\|^2\right] + 2d_m\sigma_s^2 + \frac{L^2}{2}\lambda^2d_m^3) + \frac{P}{B}C^2d_m \\ &\quad - \frac{(1-P)^2}{B}\mathbb{E}\left[\|\nabla_{w_m}F_\lambda(\mathbf{w}^t)\|^2\right] + \sigma_{dp}^2d_m \end{aligned} \quad (33)$$

Proof. First we show that the expectation on $\check{G}_m^t(\mathbf{w}^t)$ can be written as:

$$\mathbb{E}_u[\check{G}_m^t(\mathbf{w}^t)] = \frac{1}{B}\sum_{i \in \mathcal{I}_m^{t_m}}\mathbb{E}[\check{g}_{m,i}^t(\mathbf{w}^t)] + \mathbb{E}[z_m^t\mathbf{u}_m^t] = (1-P)\nabla_{w_m}F_\lambda(\mathbf{w}^t)$$

Thus, the variance can be bounded by:

$$\begin{aligned} \text{Var}(\check{G}_m^t(\mathbf{w}^t)) &= \mathbb{E}\left[\left\|\check{G}_m^t(\mathbf{w}^t) - (1-P)\nabla_{w_m}F_\lambda(\mathbf{w}^t)\right\|^2\right] \\ &= \mathbb{E}\left[\left\|\frac{1}{B}\sum_{i \in \mathcal{I}_m^{t_m}}(\check{g}_{m,i}^t(\mathbf{w}^t) - (1-P)\nabla_{w_m}F_\lambda^t(\mathbf{w}^t)) + z_m^t\mathbf{u}_m^t\right\|^2\right] \\ &= \frac{1}{B^2}\sum_{i \in \mathcal{I}_m^{t_m}}\mathbb{E}\left[\left\|\check{g}_{m,i}^t(\mathbf{w}^t) - (1-P)\nabla_{w_m}F_\lambda^t(\mathbf{w}^t)\right\|^2\right] + \mathbb{E}\left[\|z_m^t\mathbf{u}_m^t\|^2\right] \\ &\stackrel{(a)}{\leq} \frac{1-P}{B}(2d_m\mathbb{E}\left[\|\nabla_{w_m}F(\mathbf{w}^t)\|^2\right] + 2d_m\sigma_s^2 + \frac{L^2}{2}\lambda^2d_m^3) + \frac{P}{B}C^2d_m - \frac{(1-P)^2}{B}\mathbb{E}\left[\|\nabla_{w_m}F_\lambda(\mathbf{w}^t)\|^2\right] + \sigma_{dp}^2d_m, \end{aligned}$$

where (a) follows from (32). \square

B. Proof of Intermediate Lemmas

Lemma A.11 (Restatement of Lemma V.9). *Under Assumption A.1 to A.4, we have the following lemma:*

$$\begin{aligned} \mathbb{E} [F(\mathbf{w}^{t+1}) - F(\mathbf{w}^t)] &\leq - \sum_{m=0}^M q_m \eta_m (1-P) \left(\frac{1}{4} - \frac{\eta_m L(B+8d_m)}{2B} \right) \mathbb{E} [\|\nabla_{w_m} F(\mathbf{w}^t)\|^2] \\ &\quad + \sum_{m=0}^M q_m \eta_m L \left(\frac{1}{2} + 2\eta_m L^2 \right) \mathbb{E} [\|\tilde{\chi}^t - \chi^t\|^2] + \mathcal{A}_1 \end{aligned} \quad (34)$$

Proof. By assumption A.2:

$$\begin{aligned} F_\lambda(\mathbf{w}^{t+1}) &\leq F_\lambda(\mathbf{w}^t) + \langle \nabla_{\mathbf{w}} F_\lambda(\mathbf{w}^t), \mathbf{w}^{t+1} - \mathbf{w}^t \rangle + \frac{L}{2} \|\mathbf{w}^{t+1} - \mathbf{w}^t\|^2 \\ &= F_\lambda(\mathbf{w}^t) - \eta_0 \langle \nabla_{w_0} F_\lambda(\mathbf{w}^t), \check{G}_0^t(\tilde{\mathbf{w}}^t) \rangle + \frac{L\eta_0^2}{2} \|\check{G}_0^t(\tilde{\mathbf{w}}^t)\|^2 \\ &\quad - \eta_m \langle \nabla_{w_m} F_\lambda(\mathbf{w}^t), \check{G}_m^t(\tilde{\mathbf{w}}^t) \rangle + \frac{L\eta_m^2}{2} \|\check{G}_m^t(\tilde{\mathbf{w}}^t)\|^2 \\ \mathbb{E} [F_\lambda(\mathbf{w}^{t+1})] &\leq \mathbb{E} [F_\lambda(\mathbf{w}^t)] - \underbrace{\eta_0 \mathbb{E} \langle \nabla_{w_0} F_\lambda(\mathbf{w}^t), \check{G}_0^t(\tilde{\mathbf{w}}^t) \rangle}_{\mathcal{E}_1} + \underbrace{\frac{L\eta_0^2}{2} \mathbb{E} [\|\check{G}_0^t(\tilde{\mathbf{w}}^t)\|^2]}_{\mathcal{E}_2} \\ &\quad - \underbrace{\eta_m \mathbb{E} \langle \nabla_{w_m} F_\lambda(\mathbf{w}^t), \check{G}_m^t(\tilde{\mathbf{w}}^t) \rangle}_{\mathcal{E}_3} + \underbrace{\frac{L\eta_m^2}{2} \mathbb{E} [\|\check{G}_m^t(\tilde{\mathbf{w}}^t)\|^2]}_{\mathcal{E}_4} \end{aligned} \quad (35)$$

where in the second step we take expectation on both sides, first w.r.t. the random direction u , DP noise z , and the clipping event Q , then w.r.t the device m_k . We bound \mathcal{E}_1 as the following:

$$\begin{aligned} &- \eta_0 \mathbb{E} \langle \nabla_{w_0} F_\lambda(\mathbf{w}^t), \check{G}_0^t(\tilde{\mathbf{w}}^t) \rangle \\ &= -\eta_0 \mathbb{E} \langle \nabla_{w_0} F_\lambda(\mathbf{w}^t), \check{G}_0^t(\tilde{\mathbf{w}}^t) - (1-P)\nabla_{w_0} F_\lambda(\tilde{\mathbf{w}}^t) + (1-P)\nabla_{w_0} F_\lambda(\mathbf{w}^t) \rangle \\ &= -\eta_0 \mathbb{E} \langle \nabla_{w_0} F_\lambda(\mathbf{w}^t), \check{G}_0^t(\tilde{\mathbf{w}}^t) - (1-P)\nabla_{w_0} F_\lambda(\tilde{\mathbf{w}}^t) \rangle \\ &\quad - \eta_0 \mathbb{E} \langle \nabla_{w_0} F_\lambda(\mathbf{w}^t), (1-P)\nabla_{w_0} F_\lambda(\tilde{\mathbf{w}}^t) - (1-P)\nabla_{w_0} F_\lambda(\mathbf{w}^t) + (1-P)\nabla_{w_0} F_\lambda(\mathbf{w}^t) \rangle \\ &\stackrel{1)}{=} - (1-P)\eta_0 \mathbb{E} \langle \nabla_{w_0} F_\lambda(\mathbf{w}^t), \nabla_{w_0} F_\lambda(\tilde{\mathbf{w}}^t) - \nabla_{w_0} F_\lambda(\mathbf{w}^t) \rangle \\ &\quad - \eta_0 \mathbb{E} \langle \nabla_{w_0} F_\lambda(\mathbf{w}^t), (1-P)\nabla_{w_0} F_\lambda(\mathbf{w}^t) \rangle \\ &\stackrel{2)}{\leq} \frac{(1-P)\eta_0}{2} \mathbb{E} [\|\nabla_{w_0} F_\lambda(\mathbf{w}^t)\|^2] + \frac{(1-P)\eta_0}{2} \mathbb{E} [\|\nabla_{w_0} F_\lambda(\tilde{\mathbf{w}}^t) - \nabla_{w_0} F_\lambda(\mathbf{w}^t)\|^2] - (1-P)\eta_0 \mathbb{E} [\|\nabla_{w_0} F_\lambda(\mathbf{w}^t)\|^2] \\ &\stackrel{3)}{\leq} - \frac{(1-P)\eta_0}{2} \mathbb{E} [\|\nabla_{w_0} F_\lambda(\mathbf{w}^t)\|^2] + \frac{\eta_0 L}{2} \mathbb{E} [\|\tilde{\chi}^t - \chi^t\|^2] \end{aligned} \quad (36)$$

where in 1) we use the fact that $\mathbb{E} [\check{G}_0^t(\tilde{\mathbf{w}}^t) - (1-P)\nabla_{w_0} F_\lambda(\tilde{\mathbf{w}}^t)] = 0$, in 2) we applied the Cauchy–Schwarz inequality, and 3) follows by the smoothness of F_λ and the fact that $1-P \leq 1$

For \mathcal{E}_2 , we can further bound it based on Assumption A.2:

$$\begin{aligned} &\frac{1}{2} \mathbb{E} [\|\check{G}_0^t(\tilde{\mathbf{w}}^t)\|^2] \\ &= \frac{1}{2} \mathbb{E} [\|\check{G}_0^t(\tilde{\mathbf{w}}^t) - (1-P)\nabla_{x_0} F_\lambda(\mathbf{w}^t) + (1-P)\nabla_{x_0} F_\lambda(\mathbf{w}^t)\|^2] \\ &\stackrel{1)}{\leq} \mathbb{E} [\|\check{G}_0^t(\tilde{\mathbf{w}}^t) - (1-P)\nabla_{x_0} F_\lambda(\mathbf{w}^t)\|^2] + (1-P)^2 \mathbb{E} [\|\nabla_{x_0} F_\lambda(\mathbf{w}^t)\|^2] \\ &= \mathbb{E} [\|\check{G}_0^t(\tilde{\mathbf{w}}^t) - (1-P)\nabla_{x_0} F_\lambda(\tilde{\mathbf{w}}^t) + (1-P)\nabla_{x_0} F_\lambda(\tilde{\mathbf{w}}^t) - (1-P)\nabla_{x_0} F_\lambda(\mathbf{w}^t)\|^2] \\ &\quad + (1-P)^2 \mathbb{E} [\|\nabla_{x_0} F_\lambda(\mathbf{w}^t)\|^2] \\ &\stackrel{2)}{\leq} 2 \mathbb{E} [\|\check{G}_0^t(\tilde{\mathbf{w}}^t) - (1-P)\nabla_{x_0} F_\lambda(\tilde{\mathbf{w}}^t)\|^2] + 2(1-P)^2 \mathbb{E} [\|\nabla_{x_0} F_\lambda(\tilde{\mathbf{w}}^t) - \nabla_{x_0} F_\lambda(\mathbf{w}^t)\|^2] \\ &\quad + (1-P)^2 \mathbb{E} [\|\nabla_{x_0} F_\lambda(\mathbf{w}^t)\|^2] \end{aligned}$$

$$\begin{aligned}
&\stackrel{3)}{\leq} \frac{2(1-P)}{B} (2d_0 \mathbb{E} [\|\nabla_{x_0} F(\mathbf{w}^t)\|^2] + 2d_0 \sigma_s^2 + \frac{L^2}{2} \lambda^2 d_0^3) + \frac{2P}{B} C^2 d_0 \\
&\quad - \frac{2(1-P)^2}{B} \mathbb{E} [\|\nabla_{x_0} F_\lambda(\mathbf{w}^t)\|^2] + 2\sigma_{dp}^2 d_0 + 2(1-P)^2 L^2 \mathbb{E} [\|\tilde{\chi}^t - \chi^t\|^2] + (1-P)^2 \mathbb{E} [\|\nabla_{x_0} F_\lambda(\mathbf{w}^t)\|^2] \\
&\stackrel{4)}{\leq} \frac{4(1-P)d_0}{B} \mathbb{E} [\|\nabla_{x_0} F(\mathbf{w}^t)\|^2] + (1-P) \mathbb{E} [\|\nabla_{x_0} F_\lambda(\mathbf{w}^t)\|^2] + 2L^2 \mathbb{E} [\|\tilde{\chi}^t - \chi^t\|^2] + \mathcal{G}_0
\end{aligned} \tag{37}$$

where in 1) and 2) we applied the Cauchy–Schwarz inequality, and in 3) we substitute (17) in and use the L -smoothness of F_λ , and in (iv) we use the fact that $1 - P \leq 1$ and let

$$\mathcal{G}_0 = \frac{4}{B} d_0 \sigma_s^2 + \frac{L^2}{B} \lambda^2 d_0^3 + \frac{2P}{B} C^2 d_0 + 2\sigma_{dp}^2 d_0$$

Similarly, For \mathcal{E}_3 :

$$-\eta_{m_k} \mathbb{E} \langle \nabla_{w_{m_k}} F_\lambda(\mathbf{w}^t), \check{G}_m^t(\tilde{\mathbf{w}}^t) \rangle \leq -\frac{(1-P)\eta_{m_k}}{2} \mathbb{E} [\|\nabla_{w_{m_k}} F_\lambda(\mathbf{w}^t)\|^2] + \frac{\eta_{m_k} L}{2} \mathbb{E} [\|\tilde{\chi}^t - \chi^t\|^2] \tag{38}$$

And for \mathcal{E}_4 :

$$\frac{1}{2} \mathbb{E} [\|\check{G}_{m_k}^t(\tilde{\mathbf{w}}^t)\|^2] \leq \frac{4(1-P)d_m}{B} \mathbb{E} [\|\nabla_{w_{m_k}} F(\mathbf{w}^t)\|^2] + (1-P) \mathbb{E} [\|\nabla_{w_{m_k}} F_\lambda(\mathbf{w}^t)\|^2] \tag{39}$$

$$+ 2L^2 \mathbb{E} [\|\tilde{\chi}^t - \chi^t\|^2] + \mathcal{G}_m \tag{40}$$

where we let

$$\mathcal{G}_m = \frac{4}{B} d_m \sigma_s^2 + \frac{L^2}{B} \lambda^2 d_m^3 + \frac{2P}{B} C^2 d_m + 2\sigma_{dp}^2 d_m \tag{41}$$

Substituting (36), (37), (38), and (40) into (35), we have

$$\begin{aligned}
&\mathbb{E} [F(\mathbf{w}^{t+1}) - F(\mathbf{w}^t)] \\
&\leq \mathbb{E} [F_\lambda(\mathbf{w}^t)] - \frac{(1-P)\eta_0}{2} \mathbb{E} [\|\nabla_{w_0} F_\lambda(\mathbf{w}^t)\|^2] + \frac{\eta_0 L}{2} \mathbb{E} [\|\tilde{\chi}^t - \chi^t\|^2] \\
&\quad + \frac{4(1-P)d_0 L \eta_0^2}{B} \mathbb{E} [\|\nabla_{w_0} F(\mathbf{w}^t)\|^2] + (1-P) L \eta_0^2 \mathbb{E} [\|\nabla_{w_0} F_\lambda(\mathbf{w}^t)\|^2] + 2L^3 \eta_0^2 \mathbb{E} [\|\tilde{\chi}^t - \chi^t\|^2] + L \eta_0^2 \mathcal{G}_0 \\
&\quad - \frac{(1-P)\eta_{m_k}}{2} \mathbb{E} [\|\nabla_{w_{m_k}} F_\lambda(\mathbf{w}^t)\|^2] + \frac{\eta_{m_k} L}{2} \mathbb{E} [\|\tilde{\chi}^t - \chi^t\|^2] \\
&\quad + \frac{4(1-P)d_{m_k} L \eta_{m_k}^2}{B} \mathbb{E} [\|\nabla_{w_{m_k}} F(\mathbf{w}^t)\|^2] + (1-P) L \eta_{m_k}^2 \mathbb{E} [\|\nabla_{w_{m_k}} F_\lambda(\mathbf{w}^t)\|^2] \\
&\quad + 2L^3 \eta_{m_k}^2 \mathbb{E} [\|\tilde{\chi}^t - \chi^t\|^2] + L \eta_{m_k}^2 \mathcal{G}_m \\
&\leq \mathbb{E} [F_\lambda(\mathbf{w}^t)] - \eta_0 (1-P) \left(\frac{1}{2} - \eta_0 L \right) \mathbb{E} [\|\nabla_{w_0} F_\lambda(\mathbf{w}^t)\|^2] + \eta_0 L \left(\frac{1}{2} + 2\eta_0 L^2 \right) \mathbb{E} [\|\tilde{\chi}^t - \chi^t\|^2] \\
&\quad + \eta_0^2 \frac{4(1-P)d_0 L}{B} \mathbb{E} [\|\nabla_{w_0} F(\mathbf{w}^t)\|^2] + \eta_0^2 L \mathcal{G}_0 \\
&\quad - \sum_{m=1}^M q_m \eta_m (1-P) \left(\frac{1}{2} - \eta_m L \right) \mathbb{E} [\|\nabla_{w_m} F_\lambda(\mathbf{w}^t)\|^2] + \sum_{m=1}^M q_m \eta_m L \left(\frac{1}{2} + 2\eta_m L^2 \right) \mathbb{E} [\|\tilde{\chi}^t - \chi^t\|^2] \\
&\quad + \sum_{m=1}^M q_m \eta_m^2 \frac{4(1-P)d_m L}{B} \mathbb{E} [\|\nabla_{w_m} F(\mathbf{w}^t)\|^2] + \sum_{m=1}^M q_m \eta_m^2 L \mathcal{G}_m
\end{aligned} \tag{42}$$

where in the last inequality we further take expectation w.r.t. device M and combine similar terms.

From (42), we utilize the properties of the smooth function (14) and (29) to turn all the smooth function F_λ into the true loss function F :

$$\begin{aligned}
&\mathbb{E} [F(\mathbf{w}^{t+1}) - F(\mathbf{w}^t)] \stackrel{1)}{\leq} \mathbb{E} [F_\lambda(\mathbf{w}^{t+1}) - F_\lambda(\mathbf{w}^t)] + L \lambda^2 d \\
&\stackrel{2)}{\leq} -\eta_0 (1-P) \left(\frac{1}{2} - \eta_0 L \right) \left(\frac{1}{2} \mathbb{E} [\|\nabla_{x_0} F(\mathbf{w}^t)\|^2] - \frac{L^2}{4} \lambda^2 d_0^3 \right) + \eta_0 L \left(\frac{1}{2} + 2\eta_0 L^2 \right) \mathbb{E} [\|\tilde{\chi}^t - \chi^t\|^2] \\
&\quad + \eta_0^2 \frac{4(1-P)d_0 L}{B} \mathbb{E} [\|\nabla_{x_0} F(\mathbf{w}^t)\|^2] + \eta_0^2 L \mathcal{G}_0
\end{aligned}$$

$$\begin{aligned}
& - \sum_{m=1}^M q_m \eta_m (1-P) \left(\frac{1}{2} - \eta_m L \right) \left(\frac{1}{2} \mathbb{E} \left[\|\nabla_{w_m} F(\mathbf{w}^t)\|^2 \right] - \frac{L^2}{4} \lambda^2 d_m^3 \right) \\
& + \sum_{m=1}^M q_m \eta_m L \left(\frac{1}{2} + 2\eta_m L^2 \right) \mathbb{E} \left[\|\tilde{\chi}^t - \chi^t\|^2 \right] \\
& + \sum_{m=1}^M q_m \eta_m^2 \frac{4(1-P)d_m L}{B} \mathbb{E} \left[\|\nabla_{w_m} F(\mathbf{w}^t)\|^2 \right] + \sum_{m=1}^M q_m \eta_m^2 L \mathcal{G}_m + L \lambda^2 d \\
& \stackrel{3)}{\leq} - \sum_{m=0}^M q_m \eta_m (1-P) \left(\frac{1}{4} - \frac{\eta_m L(B+8d_m)}{2B} \right) \mathbb{E} \left[\|\nabla_{w_m} F(\mathbf{w}^t)\|^2 \right] \\
& + \sum_{m=0}^M q_m \eta_m L \left(\frac{1}{2} + 2\eta_m L^2 \right) \mathbb{E} \left[\|\tilde{\chi}^t - \chi^t\|^2 \right] + \sum_{m=0}^M q_m \eta_m \left(\frac{1}{2} - \eta_m L \right) \frac{L^2}{4} \lambda^2 d_m^3 \\
& + \sum_{m=0}^M q_m \eta_m^2 L \mathcal{G}_m + L \lambda^2 d \\
& \stackrel{4)}{\leq} - \sum_{m=0}^M q_m \eta_m (1-P) \left(\frac{1}{4} - \frac{\eta_m L(B+8d_m)}{2B} \right) \mathbb{E} \left[\|\nabla_{w_m} F(\mathbf{w}^t)\|^2 \right] \\
& + \sum_{m=0}^M q_m \eta_m L \left(\frac{1}{2} + 2\eta_m L^2 \right) \mathbb{E} \left[\|\tilde{\chi}^t - \chi^t\|^2 \right] \\
& + \sum_{m=0}^M q_m \eta_m \frac{L^2}{8} \lambda^2 d_m^3 + \sum_{m=0}^M q_m \eta_m^2 L \left(\frac{4}{B} d_m \sigma_s^2 + \frac{(4-B)L^2}{4B} \lambda^2 d_m^3 + \frac{2P}{B} C^2 d_m + 2\sigma_{dp}^2 d_m \right) + L \lambda^2 d \\
& \stackrel{5)}{\leq} - \sum_{m=0}^M q_m \eta_m (1-P) \left(\frac{1}{4} - \frac{\eta_m L(B+8d_m)}{2B} \right) \mathbb{E} \left[\|\nabla_{w_m} F(\mathbf{w}^t)\|^2 \right] \\
& + \sum_{m=0}^M q_m \eta_m L \left(\frac{1}{2} + 2\eta_m L^2 \right) \mathbb{E} \left[\|\tilde{\chi}^t - \chi^t\|^2 \right] + \mathcal{A}_1
\end{aligned} \tag{43}$$

where 1) and 2) follows from equation (14) and (29) in Lemma V.6 respectively. In 3), we let $q_0 = 1$ and combine similar terms. In 4), we substitute in (41). Lastly, in 5), we denote

$$\mathcal{A}_1 = \sum_{m=0}^M q_m \eta_m \frac{L^2}{8} \lambda^2 d_m^3 + \sum_{m=0}^M q_m \eta_m^2 L \left(\frac{4}{B} d_m \sigma_s^2 + \frac{(4-B)L^2}{4B} \lambda^2 d_m^3 + \frac{2P}{B} C^2 d_m + 2\sigma_{dp}^2 d_m \right) + L \lambda^2 d \tag{44}$$

for the convenience of notation.

We thus complete the proof. \square

Lemma A.12 (Restatement of Lemma V.10). *Under Assumption A.1-A.4, and assume the device delay τ_m is uniformly upper bounded by τ , we have the following lemma:*

$$\mathbb{E} [V^{t+1} - V^t] \leq -\frac{1-P}{8} \min_m \{q_m \eta_m\} \mathbb{E} \left[\|\nabla_{\mathbf{w}} F(\mathbf{w}^t)\|^2 \right] + \mathcal{A}_1 + \mathcal{A}_2$$

Proof. Before we give the proof of Lemma V.10, we first provide some useful facts that reveal properties of the delayed parameters.

Recall that $\tilde{\chi}^t$ denote the delayed parameters on all devices, and χ^t denote the non-delayed version. Let $\mathcal{F}_1 = \mathbb{E} \left[\|\chi^{t+1} - \chi^t\|^2 \right]$, $\mathcal{F}_2 = \mathbb{E} \left[\|\tilde{\chi}^t - \chi^t\|^2 \right]$.

For \mathcal{F}_1 :

$$\begin{aligned}
& \mathbb{E} \left[\|\chi^{t+1} - \chi^t\|^2 \right] \\
& = \eta_m^2 \mathbb{E} \left[\left\| \tilde{G}_{m_k}^t(\tilde{\mathbf{w}}^t) \right\|^2 \right] \\
& \leq \sum_{m=1}^M q_m \eta_m^2 \frac{2(1-P)d_m}{B} \mathbb{E} \left[\left\| \nabla_{w_{m_k}} F(\mathbf{w}^t) \right\|^2 \right] + \sum_{m=1}^M q_m \eta_m^2 \frac{(1-P)}{2} \mathbb{E} \left[\left\| \nabla_{w_{m_k}} F_{\lambda}(\mathbf{w}^t) \right\|^2 \right] \\
& + \sum_{m=1}^M q_m \eta_m^2 \left(L^2 \mathbb{E} \left[\|\tilde{\chi}^t - \chi^t\|^2 \right] + \frac{1}{2} \mathcal{G}_m \right)
\end{aligned}$$

$$\begin{aligned}
&\leq \sum_{m=1}^M q_m \eta_m^2 \frac{2(1-P)d_m}{B} \mathbb{E} \left[\left\| \nabla_{w_{m_k}} F(\mathbf{w}^t) \right\|^2 \right] + \sum_{m=1}^M q_m \eta_m^2 \frac{(1-P)}{2} \left(2\mathbb{E} \left[\left\| \nabla_{w_{m_k}} F(\mathbf{w}^t) \right\|^2 \right] + \frac{L^2}{2} \lambda^2 d_m^3 \right) \\
&+ \sum_{m=1}^M q_m \eta_m^2 \left(L^2 \mathbb{E} \left[\left\| \tilde{\chi}^t - \chi^t \right\|^2 \right] + \frac{1}{2} \mathcal{G}_m \right) \\
&= \sum_{m=1}^M q_m \eta_m^2 \frac{(1-P)(2d_m + B)}{B} \mathbb{E} \left[\left\| \nabla_{w_{m_k}} F(\mathbf{w}^t) \right\|^2 \right] + \sum_{m=1}^M q_m \eta_m^2 \left(\frac{L^2}{4} \lambda^2 d_m^3 + L^2 \mathbb{E} \left[\left\| \tilde{\chi}^t - \chi^t \right\|^2 \right] + \frac{1}{2} \mathcal{G}_m \right) \quad (45)
\end{aligned}$$

For \mathcal{F}_2 , under uniformly bounded delay, we have

$$\begin{aligned}
&\mathbb{E} \left[\left\| \tilde{\chi}^t - \chi^t \right\|^2 \right] \\
&\leq \mathbb{E} \left[\left\| \sum_{i=1}^{\tau} (\chi^{i+1} - \chi^i) \right\|^2 \right] \\
&\leq \tau \sum_{i=1}^{\tau} \mathbb{E} \left[\left\| \chi^{i+1} - \chi^i \right\|^2 \right] \quad (46)
\end{aligned}$$

where the last inequality follows by Cauchy-Schwarz Inequality.

By the definition of V^t :

$$\begin{aligned}
&\mathbb{E} \left[V^{t+1} - V^t \right] \\
&= \mathbb{E} \left[F(\mathbf{w}^{t+1}) + \sum_{i=1}^{\tau} \gamma_i \left\| \chi^{t+2-i} - \chi^{t+1-i} \right\|^2 \right] - \mathbb{E} \left[F(\mathbf{w}^t) + \sum_{i=1}^{\tau} \gamma_i \left\| \chi^{t+1-i} - \chi^{t-i} \right\|^2 \right] \\
&= \mathbb{E} \left[F(\mathbf{w}^{t+1}) - F(\mathbf{w}^t) \right] + \sum_{i=1}^{\tau} \gamma_i \mathbb{E} \left[\left\| \chi^{t+2-i} - \chi^{t+1-i} \right\|^2 \right] - \sum_{i=1}^{\tau} \gamma_i \mathbb{E} \left[\left\| \chi^{t+1-i} - \chi^{t-i} \right\|^2 \right] \\
&\stackrel{1)}{\leq} - \sum_{m=0}^M q_m \eta_m (1-P) \left(\frac{1}{4} - \frac{\eta_m L(B+8d_m)}{2B} \right) \mathbb{E} \left[\left\| \nabla_{w_m} F(\mathbf{w}^t) \right\|^2 \right] \\
&+ \sum_{m=0}^M q_m \eta_m L \left(\frac{1}{2} + 2\eta_m L^2 \right) \mathbb{E} \left[\left\| \tilde{\chi}^t - \chi^t \right\|^2 \right] + \mathcal{A}_1 \\
&+ \gamma_1 \underbrace{\mathbb{E} \left[\left\| \chi^{t+1} - \chi^t \right\|^2 \right]}_{\mathcal{F}_1} + \sum_{i=1}^{\tau-1} (\gamma_{i+1} - \gamma_i) \mathbb{E} \left[\left\| \chi^{t+1-i} - \chi^{t-i} \right\|^2 \right] - \gamma_{\tau} \mathbb{E} \left[\left\| \chi^{t+1-\tau} - \chi^{t-\tau} \right\|^2 \right] \\
&\stackrel{2)}{\leq} - \sum_{m=0}^M q_m \eta_m (1-P) \left(\frac{1}{4} - \frac{\eta_m L(B+8d_m)}{2B} \right) \mathbb{E} \left[\left\| \nabla_{w_m} F(\mathbf{w}^t) \right\|^2 \right] \\
&+ \sum_{m=0}^M q_m \eta_m L \left(\frac{1}{2} + 2\eta_m L^2 \right) \mathbb{E} \left[\left\| \tilde{\chi}^t - \chi^t \right\|^2 \right] + \mathcal{A}_1 \\
&+ \sum_{m=1}^M q_m \eta_m^2 \gamma_1 \frac{(1-P)(2d_m + B)}{B} \mathbb{E} \left[\left\| \nabla_{w_{m_k}} F(\mathbf{w}^t) \right\|^2 \right] + \sum_{m=1}^M q_m \eta_m^2 \gamma_1 \left(\frac{L^2}{4} \lambda^2 d_m^3 + L^2 \mathbb{E} \left[\left\| \tilde{\chi}^t - \chi^t \right\|^2 \right] + \frac{1}{2} \mathcal{G}_m \right) \\
&+ \sum_{i=1}^{\tau-1} (\gamma_{i+1} - \gamma_i) \mathbb{E} \left[\left\| \chi^{t+1-i} - \chi^{t-i} \right\|^2 \right] - \gamma_{\tau} \mathbb{E} \left[\left\| \chi^{t+1-\tau} - \chi^{t-\tau} \right\|^2 \right] \\
&\stackrel{3)}{=} - \eta_0 (1-P) \left(\frac{1}{4} - \frac{\eta_0 L(B+8d_0)}{2B} \right) \mathbb{E} \left[\left\| \nabla_{x_0} F(\mathbf{w}^t) \right\|^2 \right] \\
&- \sum_{m=1}^M q_m \eta_m (1-P) \left(\frac{1}{4} - \frac{\eta_m L(B+8d_m)}{2B} - \frac{\eta_m \gamma_1 (2d_m + B)}{B} \right) \mathbb{E} \left[\left\| \nabla_{w_m} F(\mathbf{w}^t) \right\|^2 \right] \\
&+ \left\{ \eta_0 L \left(\frac{1}{2} + 2\eta_0 L^2 \right) + \sum_{m=1}^M q_m \eta_m L \left(\frac{1}{2} + 2\eta_m L^2 + \eta_m \gamma_1 L \right) \right\} \underbrace{\mathbb{E} \left[\left\| \tilde{\chi}^t - \chi^t \right\|^2 \right]}_{\mathcal{F}_2} \\
&+ \mathcal{A}_1 + \sum_{m=1}^M q_m \eta_m^2 \gamma_1 \left(\frac{L^2}{4} \lambda^2 d_m^3 + \frac{1}{2} \mathcal{G}_m \right)
\end{aligned}$$

$$\begin{aligned}
& + \sum_{i=1}^{\tau-1} (\gamma_{i+1} - \gamma_i) \mathbb{E} \left[\|\chi^{t+1-i} - \chi^{t-i}\|^2 \right] - \gamma_\tau \mathbb{E} \left[\|\chi^{t+1-\tau} - \chi^{t-\tau}\|^2 \right] \\
& \stackrel{4)}{\leq} -\eta_0(1-P) \left(\frac{1}{4} - \frac{\eta_0 L(B+8d_0)}{2B} \right) \mathbb{E} \left[\|\nabla_{x_0} F(\mathbf{w}^t)\|^2 \right] \\
& - \sum_{m=1}^M q_m \eta_m (1-P) \left(\frac{1}{4} - \frac{\eta_m L(B+8d_m)}{2B} - \frac{\eta_m \gamma_1 (2d_m+B)}{B} \right) \mathbb{E} \left[\|\nabla_{w_m} F(\mathbf{w}^t)\|^2 \right] \\
& + \sum_{i=1}^{\tau-1} \left(\gamma_{i+1} - \gamma_i + \tau \left(\eta_0 L \left(\frac{1}{2} + 2\eta_0 L^2 \right) + \sum_{m=1}^M q_m \eta_m L \left(\frac{1}{2} + 2\eta_m L^2 + \eta_m \gamma_1 L \right) \right) \right) \mathbb{E} \left[\|\chi^{t+1-i} - \chi^{t-i}\|^2 \right] \\
& - \left(\gamma_\tau - \tau \left(\eta_0 L \left(\frac{1}{2} + 2\eta_0 L^2 \right) + \sum_{m=1}^M q_m \eta_m L \left(\frac{1}{2} + 2\eta_m L^2 + \eta_m \gamma_1 L \right) \right) \right) \mathbb{E} \left[\|\chi^{t+1-\tau} - \chi^{t-\tau}\|^2 \right] \\
& + \mathcal{A}_1 + \mathcal{A}_2. \tag{47}
\end{aligned}$$

Above, we used Lemma V.9 in step (1), substituted in (45) for \mathcal{F}_1 in step (2), substituted in (46) for \mathcal{F}_2 in step (3), and defined

$$\begin{aligned}
\mathcal{A}_2 &:= \sum_{m=1}^M q_m \eta_m^2 \gamma_1 \left(\frac{L^2}{4} \lambda^2 d_m^3 + \frac{1}{2} \mathcal{G}_m \right) \\
&= \sum_{m=1}^M q_m \eta_m^2 \gamma_1 \left(\frac{L^2}{4} \lambda^2 d_m^3 + \frac{2}{B} d_m \sigma_s^2 + \frac{L^2}{2B} \lambda^2 d_m^3 + \frac{P}{B} C^2 d_m + \sigma_{dp}^2 d_m \right). \tag{48}
\end{aligned}$$

From (47), we choose the following relationship for $\gamma_1, \gamma_2, \dots, \gamma_m$:

$$\begin{aligned}
\gamma_1 &= \frac{\tau^2 \left(\eta_0 L \left(\frac{1}{2} + 2\eta_0 L^2 \right) + \sum_{m=1}^M q_m \eta_m L \left(\frac{1}{2} + 2\eta_m L^2 \right) \right)}{1 - \tau^2 \sum_{m=1}^M q_m \eta_m^2 L^2} \\
\gamma_{i+1} &= \gamma_i - \tau \left(\eta_0 L \left(\frac{1}{2} + 2\eta_0 L^2 \right) + \sum_{m=1}^M q_m \eta_m L \left(\frac{1}{2} + 2\eta_m L^2 + \eta_m \gamma_1 L \right) \right)
\end{aligned} \tag{49}$$

and we can verify that

$$\gamma_\tau - \tau \left(\eta_0 L \left(\frac{1}{2} + 2\eta_0 L^2 \right) + \sum_{m=1}^M q_m \eta_m L \left(\frac{1}{2} + 2\eta_m L^2 + \eta_m \gamma_1 L \right) \right) \geq 0$$

We further let

$$\eta_0 \leq \frac{B}{4L(B+8d_0)}, \eta_m \leq \frac{B}{4L(B+8d_0) + 8\gamma_1(2d_m+B)},$$

and we finally have

$$\begin{aligned}
\mathbb{E} [V^{t+1} - V^t] &\leq -\frac{\eta_0}{8}(1-P) \mathbb{E} \left[\|\nabla_{x_0} F(\mathbf{w}^t)\|^2 \right] - \sum_{m=1}^M \frac{q_m \eta_m}{8}(1-P) \mathbb{E} \left[\|\nabla_{w_m} F(\mathbf{w}^t)\|^2 \right] + \mathcal{A}_1 + \mathcal{A}_2 \\
&\leq -\frac{1-P}{8} \min_m q_m \eta_m \mathbb{E} \left[\|\nabla_{\mathbf{w}} F(\mathbf{w}^t)\|^2 \right] + \mathcal{A}_1 + \mathcal{A}_2 \tag{50}
\end{aligned}$$

which completes the proof. \square

C. Additional Details on Experiment

In this section, we would like to give a brief introduction of the datasets and model structures and further justify the choice of the experimental designs below. We follow the experimental settings of existing works [2], [3], [22] for a fair comparison.

Dataset The choices of datasets cover a large range of tasks, including:

- MNIST and CIFAR-10: standard image benchmarks in machine learning.
- ModelNet40: multi-view 3D object classification dataset; each object has 12 views from different angles, which naturally lends itself to feature partitioning across devices in VFL.
- Amazon Reviews: sentiment analysis task, which we include to evaluate our algorithm in the NLP domain.

Data partition and model selection For MNIST, we use a two-layer CNN model, for VFL's data partitioning, we split the images by row evenly into 7 sub-images and assign them to 7 devices. For CIFAR-10 we use a four-layer CNN model, and

partition each image into 2×2 , 4 patches of the same size for 4 devices. For ModelNet40, we use a ResNet-18 model, and partition each object into 12 different camera views and allocate them to 12 devices. For Amazon Reviews, we use a pre-trained BERT [48] model, and split the tokenized data input into 3 paragraphs of the same number of tokens and distributed them across 3 devices. For all four datasets, we use a fully connected model of two linear layers with ReLU activations as the server model.